COASTAL TRAPPED WAVES GENERATED BY HURRICANE ANDREW ON THE TEXAS-LOUISIANA SHELF

A Thesis

by

STUART MICHAEL PEARCE

Submitted to the Office of Graduate Studies of
Texas A&M University
in partial fulfillment of the requirements for the degree of

MASTER OF SCIENCE

December 2011

Major Subject: Oceanography

COASTAL TRAPPED WAVES GENERATED BY HURRICANE ANDREW ON THE TEXAS-LOUISIANA SHELF

A Thesis

by

STUART MICHAEL PEARCE

Submitted to the Office of Graduate Studies of
Texas A&M University
in partial fulfillment of the requirements for the degree of

MASTER OF SCIENCE

Approved by:

Chair of Committee,	Steven F. DiMarco
Committee Members,	David A. Brooks
	Courtney Schumacher
Head of Department,	Piers Chapman

December 2011

Major Subject: Oceanography

ABSTRACT

Coastal Trapped Waves Generated by Hurricane Andrew on
the Texas-Louisiana Shelf. (December 2011)
Stuart Michael Pearce, B.S., Auburn University
Chair of Advisory Committee: Dr. Steven F. DiMarco

The Texas-Louisiana Shelf Circulation and Transport Study featured moorings that covered the shelf during 1992 to 1994, and captured the oceanic response on the shelf to category 4 Hurricane Andrew in August of 1992. Eighty-one current meters distributed over 31 moorings along several contours of isobaths provided excellent spatial and temporal coverage over the shelf. The low-frequency variability (2 days and longer) of current observations and tide gauges to the West of the storm are analyzed after the passage of Andrew, focusing on the region outside of direct hurricane forcing. Wavelet analyses are utilized to investigate the dominant periods excited by the storm over the shelf and their temporal evolution after forcing has subsided. Subsequent to the storm's passage, the observations and wavelet transforms show a two-to-four day period coastal trapped wave that propagate westward at speeds near 6 m/s and then around the Texas bend along the bathymetry. The signal remains detectable in observations as far south as Port Isabel, Texas. The prominent frequencies determined from wavelet analysis are compared with predicted coastal trapped wave dispersion modes and show good agreement in the predicted group speed and cross-shelf structure of the first mode. The energies calculated from the data indicate a largely barotropic shelf wave response which is corroborated in the observed currents and by theory.

To my Uncle, Rick Pearce, who in part inspired me to pursue science.

ACKNOWLEDGMENTS

I am grateful to my committee Drs. Steven DiMarco, David Brooks, and Courtney Schumacher and to Dr. Rob Korty for substituting for my defense. Additionally I would like to thank Drs. David C. Smith IV, Matt Howard, and Rob Hetland for advice and discussions; Drs. Christopher Torrence and Gilbert Compo for the use of their Wavelet package (available at http://paos.colorado.edu/research/wavelets/); and to Dr. Ken Brink for both his Coastal Trapped Wave program and for listening and providing helpful advice. I am especially grateful to both Nancy Scarlett Arbuckle and Chris Paul for helpful suggestions and discussions.

LATEX Program data provided by the U.S. Minerals Management Service contract no. 14-35-0001-30509

TABLE OF CONTENTS

LIST OF TABLES

LIST OF FIGURES

CHAPTER I

INTRODUCTION

Hurricane Andrew crossed over the Texas-Louisiana Shelf in August of 1992 affecting the ocean dynamics of the entire shelf. Theory predicts that a major response to a moving cyclonic storm beyond the forcing winds is a coastal trapped wave, whose response is confined to the shelf and slope and decays out to open ocean [*Tang and Grimshaw*, 1995; *Tang et al.*, 1997]. Based on the spatial and temporal scales of Hurricane Andrew and characteristics of the shelf, the response was indeed likely in the form of a coastal trapped wave. At the time, a mooring array and several tidal stations existed on the shelf and provided good observation of the neritic response to the west outside of hurricane forcing where a trapped wave would propagate freely. The following is a study of the data available and a determination of the likelihood of a free trapped wave response.

Waves have long been a topic of studies that have been historically performed by physicists and mathematicians like Bernoulli, Laplace, Stokes, and Kelvin who searched for analytical solutions to early fluid dynamics problems. During World War II, widespread use of amphibious landing craft for beach invasion required extended knowledge of coastal waves be available to the United States government, which initiated studies at Scripps Institute of Oceanography by Harald Sverdrup and Walter Munk on the dynamics and prediction of waves [*Bigelow and Edmondson*, 1947]. This in part has led to the investigation of coastal waves and waves in general, as a subfield of physical oceanography. After World War II, recreational use of beaches became common, and the oil industry began exploration for offshore oil fields by drilling

---

The journal model is *Journal of Geophysical Research-Oceans.*

on the continental shelf, both of which increased efforts for storm surge and coastal wave prediction [*Palmer*, 1996; *Wiegel and Saville Jr.*, 1996]. This was especially true for disaster prediction due to long wavelength storm surges, such as from the Hurricane that hit Galveston, TX, in 1900, which killed approximately 6000 people [*Wiegel and Saville Jr.*, 1996]. In the 1950's, spectral techniques were developed and began playing an important role in observations of waves, which permitted a wider range of frequencies of waves to be studied [*Palmer*, 1996]. No doubt this aided in the discovery and development of understanding of coastal trapped waves, which had been previously theorized, but not well observed.

Theories developed by Kelvin and Stokes in the late nineteenth century found that trapping mechanisms occur from the interaction of a long wave (long wavelength compared to the depth) with the coast. These waves, trapped in the presence of the coast, are largest in amplitude at the coast and decay offshore, confined to propagate parallel to the shoreline. As technology and techniques advanced through the post-war era, observations of trapped waves became more prevalent and further development of the theories soon followed. There are several types of trapped wave theories that have arisen, each corresponding to an idealized situation of stratification and bottom topography: three barotropic homogenous types; barotropic Kelvin waves, edge waves, and continental shelf waves [*Huthnance*, 1975]; and two baroclinic types; internal Kelvin waves and general coastal trapped waves that are a hybrid of types [*Allen*, 1975; *Clarke*, 1977]. Barotropic Kelvin waves are large waves that lean against a coastal wall over a flat bottomed ocean and are typically large enough to generate geostrophic currents. Edge waves exist over a sloping bottom and are superinertial (i.e., the frequency ω is greater than the Coriolis parameter f, $\omega > f$). Continental shelf waves are subinertial waves ($\omega < f$) over a sloping shelf and slope that are less dictated by the gravitational restoring force and more by conservation of

potential vorticity. The baroclinic variety of Kelvin waves are similar to the barotropic variety, occurring against a coastal wall over a flat bottom; however, due to a stratified water column, isopycnals oscillate in addition to the surface. General coastal trapped waves are a result of a sloping bottom with a stratified water column, and are a hybrid of shelf waves and internal Kelvin waves. In the limit of no stratification or a flat bottom, coastal trapped waves reduce to their respective component types; an internal Kelvin or shelf wave. Further descriptions of the types are given in the sections below. Thorough reviews on the types of coastally trapped waves and their behavior can also be found in *Mysak* [1980], *Magaard and Mysak* [1986],*Brink* [1991], and *Allen* [1980].

A. Trapped Wave Types

1. Kelvin Waves

William Thomson [1879] (otherwise known as Lord Kelvin) described long (compared to depth) gravitational oscillations of the sea surface for a homogenous ocean in a flat bottomed rotating circular basin that leans against the edge of the basin (i.e the coast) and exponentially decays offshore (Figure 1); these have come to be known as Kelvin waves. The spatial and temporal scales associated with Kelvin waves are such that the Earth rotates through a significant portion or greater of its revolution, meaning that the Earth's rotation is important to the dynamics of the wave in the form of Coriolis acceleration. The Coriolis force balances out the pressure gradient at the wall due to gravity, maintaining the motions of the wave and keeping the wave against the wall [*Magaard and Mysak*, 1986]. As a result of the Coriolis balance, a Kelvin wave can only propagate in one direction; where the coast lies to the right of the direction of propagation (in the Northern Hemisphere). The phase speed has

been shown to be $c = \sqrt{gH}$, where g is the acceleration due to gravity and H is the depth; this is the same as for non-rotational shallow water gravity waves (the same as long waves, a wavelength that is greater than the depth). Baroclinic or internal Kelvin waves are similar to their barotropic/external counterpart, but are restricted to slower phase speeds and manifest themselves internally along the isopycnals due to the stratification. The internal speed is $c = \sqrt{g'h}$ where instead, g' is the reduced effect of gravity, determined by the density differences due to stratification, and h is the depth of the density layer [*LeBlond and Mysak*, 1978].

Descriptions of baroclinic Kelvin waves have been made off the coast of Peru, found propagating poleward and asserted to possibly be generated by El Niño equatorial Kelvin waves [*Smith*, 1978]. The Peru observations however, were also found to be in good agreement with general coastal trapped wave theory [*Brink*, 1982]. Though *Thomson* [1970] demonstrates that Kelvin waves can be generated on the coast by the alongshore wind component and to a lesser extent atmospheric pressure disturbances, most sources describing observations of fully barotropic Kelvin waves in the ocean are in relation to the tides. This would suggest that Kelvin waves can only exist on scales large enough to make the continental slope appear as the proverbial vertical wall, which hardly exists otherwise. The Rossby radius of deformation is the scale to which a barotropic Kelvin wave decays offshore and is given by $Ro = \sqrt{gH}/f$, where f is the Coriolis parameter (also called the inertial frequency), related to Earth's rotation by $f = 2\Omega \sin \phi$, where Ω is the angular frequency of Earth's rotation and ϕ is the latitude [*LeBlond and Mysak*, 1978]. For a deep depth of 3000 m, as in the Gulf of Mexico, and near the longitude of the Texas-Louisiana shelf at 30°N, $Ro \approx 2300$ km for a barotropic Kelvin wave, which makes a gentle sloping shelf-slope with a width of 600 km certainly appear as a wall. A baroclinic Rossby radius of deformation is the scale for an internal Kelvin wave $Ro = \sqrt{g'h}/f$, with the same parameters as for

the phase speed, is much smaller than the external counter part.

2. Edge Waves

Edge waves are long wavelength coastal trapped waves that occur in the presence of a continually sloping infinite bottom. They are similar to Kelvin waves in that the sea level response is largest at the coast and decays exponentially away from shore, within one wavelength from the coast and consist of an infinite number of cross-shelf modes[*Munk et al.*, 1956]. In contrast, they are considered to exist at frequencies greater than the local inertial frequency (superintertial) and are smaller in wavelength and decay scale than Kelvin or shelf waves, so Earth's rotation does not play as great a role as gravity. Their trapping mechanism is instead maintained by refraction[*Mysak*, 1980]. Since rotation is not as important for edge waves, they can propagate in both directions along the coast from the source of generation. However, *Reid* [1958] analyzed the effect of the coriolis parameter on edge waves and found that when the wavelength grew very large, two types of edge waves occurred, one of the normal type that propagated upcoast, and a quasigeostrophic variety that propagated downcoast like a Kelvin wave, exhibited more vorticity, and propagated with a slower phase speed. Edge waves have been shown, both analytically and observationally, to occur as a response to moving atmospheric pressure disturbances and that for large scale pressure distributions, the fundamental mode is primarily excited [*Munk et al.*, 1956; *Greenspan*, 1956; *Buchwald and Szoeke*, 1973]. *LeBlond and Mysak* [1978] demonstrate that the pressure distribution is the dominant generation mechanism of edge waves when compared to wind stress, but conclude that on typical coastal meteorological scales that wind generation can still be important.

3. Continental Shelf Waves

Continental shelf waves are long waves that occupy frequencies less than the local inertial frequency (subinertial) and like Kelvin waves have spatial and temporal scales that are large compared to Earth's rotation,

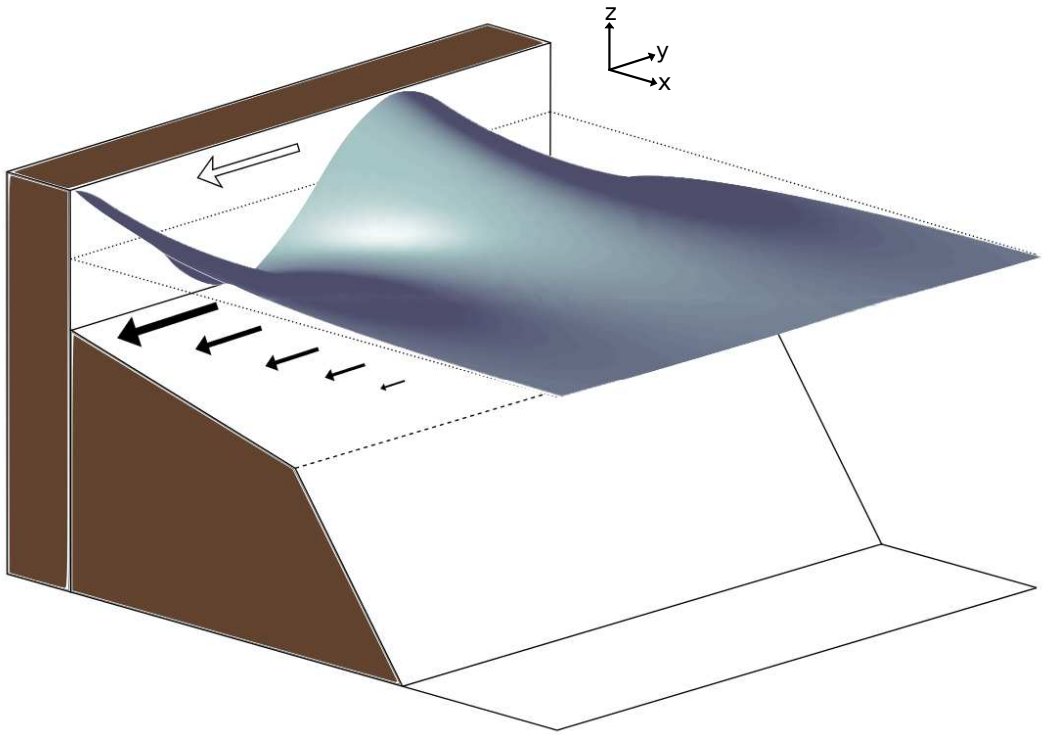

Fig. 1. A computer-assisted conception of a gravest-mode shelf wave (recreated from *Cutchin and Smith* [1973]). The white arrow along the coast indicates direction of phase propagation in the northern hemisphere and the black arrows over the shelf-slope region indicate the water velocity under the crest. The vertical displacement of the sea surface is greatly exaggerated - in the ocean, shelf-wave amplitudes are only a few centimeters

and the Coriolis acceleration becomes important to the dynamics. Unlike Kelvin waves, shelf waves are not as dependent on gravity as the restoring force, but instead

are restored by conservation of potential vorticity by the squeezing and stretching of a column of water displaced up and down the sloping shelf; thus they are highly rotational by nature and do not have as great of a surface expression ($\sim$cm)[*Mysak*, 1980]. Shelf waves also propagate, like Kelvin waves, in one direction with the coast on the right in the Northern Hemisphere.

In 1957, *Hamon* [1962] expected sea level observations off the Australian coast to act as an inverse barometer to changing atmospheric pressure systems, but instead found that some stations changed less than predicted. The anomalous sea level disturbance was also found to propagate northwards along the coast. *Robinson* [1964] then showed that a traveling sinusoidal atmospheric pressure field can excite a resonance response between the sea surface and the atmospheric pressure distribution that allows sea level to respond differently than an inverse barometer and produce waves that are confined to the coast in the presence of a finite width sloping shelf as an explanation to Hamon's observations. These trapped waves Robinson termed continental shelf waves. Since then, there have been numerous observations of continental shelf waves on the shelves of Oregon, North Carolina, Nicaragua, Australia, and Newfoundland [*Brooks*, 1978; *Cutchin and Smith*, 1973; *Dukhovskoy et al.*, 2008; *Freeland et al.*, 1986; *Mooers and Smith*, 1968; *Thiebaut and Vennell*, 2010].

Early on, continental shelf wave generation was attributed to changing distrubutions in atmospheric pressure [*Mysak*, 1967; *Robinson*, 1964]. Shortly after, variable wind stress in the alongshore wind component was revealed as being the dominant generating mechanism, over atmospheric pressure perturbations [*Adams and Buchwald*, 1969]. *Gill and Schumann* [1974] created a model to investigate the response of the coastal currents and sea level to the alongshore wind stress. Their model showed that the first cross-shelf mode of a shelf wave out of an infinite number of modes is typically the dominant expression.

4. Coastal Trapped Waves

Eventually, shelf wave theory advanced to the more general case of coastal trapped waves by including stratification [*Brink*, personal communication]. The case was first explored as a two layered water column [*Wang*, 1975; *Allen*, 1975], and then followed by the case of continuous stratification [*Huthnance*, 1978; *Wang and Mooers*, 1976]. Coastal trapped waves exist as a hybrid of internal Kelvin waves and shelf waves, exhibiting both large vorticity and some isopycnal displacement [*Allen*, 1975], remain in the subinertial range, and propagate downcoast the same as Kelvin and shelf waves. Internal Kelvin waves, and shelf waves can then be considered special cases of coastal trapped waves; where in certain limits, coastal trapped waves reduce to the two special types. In the limit of steep bathymetry with stratification, coastal trapped waves reduce to internal Kelvin waves, and in the limit of vanishing stratification, they reduce to shelf waves [*Huthnance*, 1978]. Additional investigations on coastal trapped waves have shown that in the case of wind forcing, the motion occurs as a sum of the modes [*Clarke*, 1977]. The effect of bottom friction [*Brink*, 2006], beta effect, and coastline curvature [*Grimshaw*, 1977] have also been examined.

There has been some ambiguity in the literature as to the usage of the term "coastal trapped waves". At times the term has been used to mean any wave that is confined along the coastline, and in other situations, the term is used to mean the above case of shelf and slope bottom topography with stratification. The latter situation is now taken as the appropriate one, and has been used in this manner over the more recent studies of trapped waves (1970's to present).

B. Relation to Hurricanes

Naturally, studies of coastal trapped waves generated by wind variations and atmospheric disturbances have led to studies involving intense storms impacting the coastal ocean, and in particular hurricanes and their effect. Several investigations have been made of the influence of hurricane type disturbances on the generation of coastal trapped waves [*Fandry et al.*, 1984; *Grimshaw*, 1988; *Tang and Grimshaw*, 1995; *Tang et al.*, 1997]. *Fandry et al.* [1984] reported southward propagating "Kelvin-type" surges on the western coast of Australia traveling 5–7 m/s with amplitudes of 1–2 m possibly in resonance with southward traveling tropic cyclones. *Grimshaw* [1988] extended *Gill and Shumann*'s [1974] model by allowing a Kelvin response, using the full wind stress (rather than the alongshore component), and coupling to the deep ocean through an idealized shelf-slope system. Grimshaw's extended model was applied to the case of a cyclone-like localized weather system with pressure and associated winds that moved parallel or normal to the coast; which revealed shelf waves as the dominant response to the traveling cyclone. *Tang and Grimshaw* [1995] further extended Grimshaw's description using numerical simulations to determine the modal structures generated by tropical cyclones and provide a method for fitting observations to those modes; again shelf waves of the low-modes are revealed as the dominant response to the storm. Then, *Tang et al.* [1997] examined a numerical simulation of a tropical cyclone on the western Australian coast using realistic bathymetry and coastlines and compared the results to observations of Tropical Cyclone Jane of sea level and alongshelf currents, focusing on the region away from the forcing of the storm. The response far from the storm forcing was found to be best represented by a barotropic continental shelf wave. The observation of Tropical Cyclone Jane in *Tang et al.* [1997] was similar to the observations made in the northwestern Gulf of

Mexico of Hurricane Andrew, which is used in this study. Both traveled at relatively the same rate and crossed the shelf nearly perpendicularly with observations made primarily in the downcoast direction from the storm. Below is a description of the characteristics of Hurricane Andrew.

C. Hurricane Andrew and LATEX Description

In August of 1992, Hurricane Andrew formed in the Atlantic Ocean and passed over the southern tip of Florida as a Category 5 storm (winds $>$ 249 km/h on the Saffir-Simpson wind scale), destroying parts of Miami and the surrounding area in the process. On August 24th, Andrew entered the Gulf of Mexico from Florida's tip with a translation speed of about 9 m/s and crossed the Gulf in a north-westerly arc over 2 days as a Category 4 (winds of 210–249 km/h) storm and then exited the Gulf just west of the Mississippi Delta with a translation speed of about 5 m/s [*Cardone et al.*, 1994; *Landsea et al.*, 2004]. Andrew was a relatively compact storm with a radius of maximum winds occurring at about 16 km as it entered the Gulf and about 30 km as it exited [*Cardone and Cox*, 1992]; compared to an average radius of maximum wind speeds of 48 km for category 4 hurricanes [*Hsu and Yan*, 1998]. It traversed the shelf in about 12 hours and passed over the easternmost moorings of the LATEX program.

The field component of the U.S. Minerals Management Service funded Texas-Louisiana Shelf Circulation and Transport Process Study (LATEX), occurred from April 1992 to December 1994 [*DiMarco et al.*, 1997; *Nowlin et al.*, 1998]. During this time 81 current meters distributed over 31 mooring locations recorded current velocities, temperature, and salinity. The moorings were positioned following bathymetric contours from near the Mississippi River Delta to Corpus Christi, TX through the Texas bight featuring 5 cross-shelf lines with moorings covering the 10, 20, and 50

m isobaths, and an alongshelf line following the 200 m isobath (Figure 2). Andrew passed over the easternmost portion of the LATEX moorings approaching very near moorings 14 and 15. Although several instruments malfunctioned, good measurements of the passing storm were recorded at 26 stations.

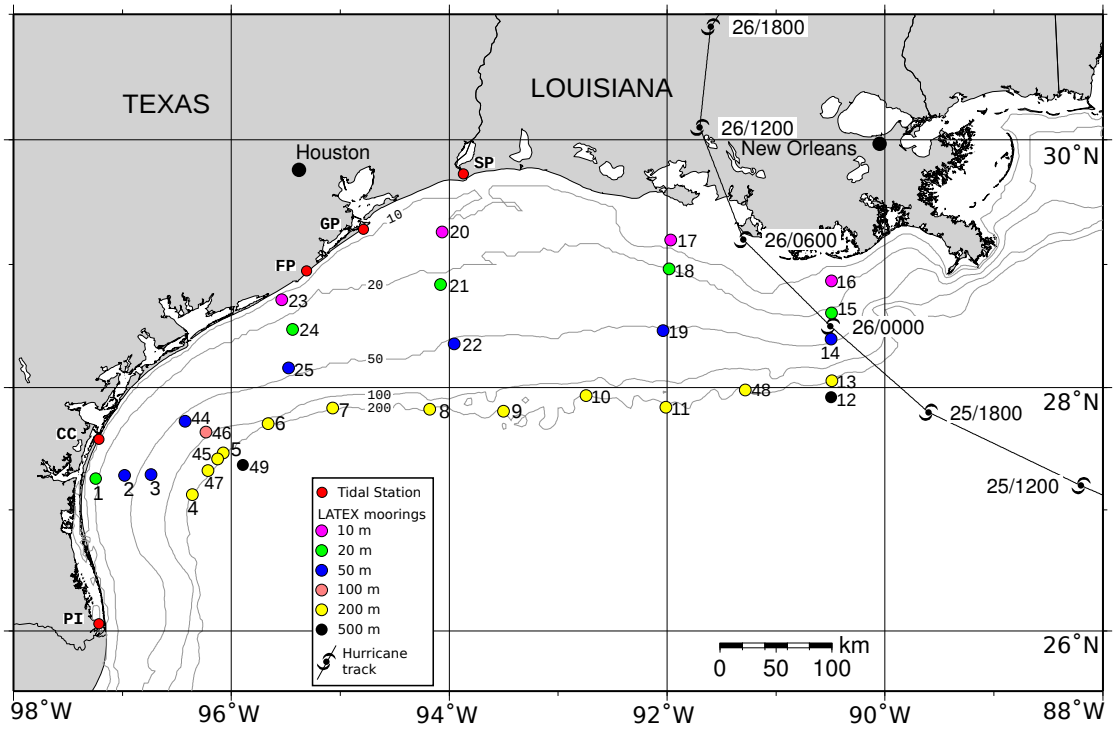

Fig. 2. LATEX Moorings and Hurricane Andrew Path in the Northwest Gulf of Mexico. The moorings are color coded according to their nominal water depths of 20, 50, 100, 200, and 500 m. The tide stations are also color coded. The color representations are used in later figures to identify the moorings along each isobath. Position times are listed next to the hurricane symbols on the storm track for August of 1992.

D. Background

Several studies have looked at Hurricane Andrew and its effect in the Gulf, such as *DiMarco et al.* [2001], which investigated nonlinear wave-wave interactions during the storm and a hindcast of the storm by *Cardone et al.* [1994]. *Keen and Glenn*

[1999] compared the hindcast results of *Cardone et al.* [1994] to the LATEX observations to investigate the importance of stratification on the dynamics of shallow water currents (turbulent mixing, trapped waves, near-inertial oscillations, and upwelling/downwelling). Following the Hurricane Andrew's exit from the Gulf, *Keen and Glenn* [1999] (here after referred to as KG99) describe the storm surge as relaxing and propagating to the west as a Kelvin wave; this is found in observations and in their Princeton Ocean Model hindcast results (the same model as *Cardone et al.* [1994]). They found the trapped Kelvin wave to be predominately barotropic generated from a combination of the relaxation of the bulge of storm surge water and a sea level gradient created by uneven wind stresses, east and west of the eye, as the storm moved onshore.

In KG99's study, the peak of the storm surge was determined using the pressure record on mooring 16 located in the right front quadrant of the storm as it passed. They determined propagation from bottom pressure data at Eugene Isle just to the west of the storm track, though due to gaps in the bottom pressure data they were unable to determine a phase speed. The theoretical phase speed, KG99 provides, is 14 m/s for an average depth of 20 m ($\sqrt{gH}$). The hindcast model gives a phase speed of the Kelvin wave as 2.8 m/s, much lower than the theoretical phase speed. KG99 attributes this to wind forcing opposing the direction of propagation following the passage of the eye. A baroclinic component was also observed from the temperature records with a phase speed of about 4 m/s measured from the time of arrival of peak temperature change between moorings.

As mentioned before, the dominant response to a translating cyclonic wind stress field is the generation of a barotropic continental shelf wave [*Tang and Grimshaw*, 1995; *Tang et al.*, 1997], and due to the highly vortical nature of shelf waves, they are best observed in the currents. Since the focus of the KG99 and *Cardone et al.*

[1994] hindcast model was on the forced response to the storm, only the easternmost moorings in the LATEX array were used and observation of a shelf wave were beyond the scope of their studies; yet the shelf exhibited a response to the storm as far downcoast as the Texas-Mexico border.

The goal of the current study is to describe the free and unforced response on the Texas-Louisiana shelf to the west of Hurricane Andrew and to provide evidence of the presence of a coastal trapped wave. The objectives to provide a convincing argument for trapped waves then are to demonstrate:

- the propagation of an oscillating signal parallel to and down the coast,
- a cross-shelf structure with amplitude largest inshore and decaying offshore,
- a surface expression,
- subinertial frequencies;

and to characterize the wave by determination or estimation of:

- the wave frequencies,
- an along-coast propagtion speed (group speed),
- a generation time and location;

and compare those characteristics to a dispersion and cross-shelf structure model. The methods used to accomplish these objectives are given in Chapter II, and the objectives imparted in Chapter III.

CHAPTER II

DATA AND METHODS

A. Data

1. LATEX Time Series

The LATEX data consists of current meter velocities, temperature, and salinity from the mooring arrangement described above from April of 1992 to December of 1994. Processing, quality assurance/quality control, and mooring configurations as well as the data availability are described in *DiMarco et al.* [1997]. The current meter velocities exist in raw and several low-passed filtered formats. The raw data are in various time steps, but most are half hour records. A cosine-Lanczos filter, which is a weighted sinc function filter [*Duchon*, 1979], was applied to the time series data to obtain a 3-hour low-passed version (3HLP), which removes high frequency signal, and a 40-hour low-passed version (40HLP), which removes the diurnal, semidiurnal, and inertial signals from the record for the latitudes involved. The filtered data were both decimated to hourly intervals for the 3HLP version and to 6-hourly and hourly intervals for the 40HLP versions.

DiMarco et al. [1997] lists the alongshore orientations for each of the LATEX moorings, which were used to transform the data to its alongshelf and cross-shelf components as described by *Emery and Thomson* [2001]. Rotation of the currents to their principle axis, was done in such a way that the positive alongshelf currents are in the direction of Louisiana, or in the upcoast direction in the sense of a downcoast propagating Kelvin wave (i.e with the coast to the right of the propagation direction).

The analysis presented here primarily focuses on the alongshelf currents of the 40HLP data due to the subinertial nature and majority of variability of a coastal

trapped wave primarily occurring in the alongshelf direction; particularly in the long wave limit where the alongshelf scales are much greater than the cross-shelf scales [*Brink*, 1991].

2. Tide Records

Six tidal stations along the Texas Coast (which extends from the Louisiana border, to the border of Mexico) were in operation during the passage of Hurricane Andrew in 1992 at Sabine Pass, Galveston, Free Port, Rock Port, Corpus Christi, and Port Isabel. The data are hourly water levels and are available at NOAA's Historic Tide Data of the Tides and Currents website: http://tidesandcurrents.noaa.gov. There the data can be downloaded as an ASCII text file and includes observed and predicted water levels for each station. The residual water levels were calculated by subtracting the NOAA predicted tides and the observed water levels at each station. After removal of the tides, the residual levels were filtered using the 40HLP cosine-Lanczos filtering scheme. The data from the Rock Port station ultimately was dropped from the analysis due to its location behind an extensive network of barrier islands and a consistent lag behind the other stations presumably from damping by the islands.

B. Methods

1. Wavelet Analysis

Since many geophysical temporal phenomena are inherently periodic, one of the most common data analysis methods involve identifying the spectral range of frequencies which are present in a time series. Typically, spectral analysis makes use of the Fourier transform which assumes stationary power or amplitude of each frequency throughout the time series [*Emery and Thomson*, 2001]. For this reason, a

temporal component is not determined by the Fourier transform, only the average power throughout the record. Many geophysical phenomenon however, are not stationary and change through time. Wavelet analysis, as described by *Torrence and Compo* [1998], uses a waveform modulated by a Gaussian curve, or wavelet, to localize the spectral analysis to moments in the time series, so non-stationary signals can be described by their power over time. The wavelet is scaled and translated, and a convolution with the dataset is performed, essentially band-pass filtering the data over multiple frequency ranges. The wavelet transform then provides a description of power as a function of period/frequency and time, showing when certain frequencies were activated during the time series record.

Wavelet analysis has only recently been introduced to Oceanography and Meteorology [*Meyers et al.*, 1993]; and although relatively new, has already been incorporated into many geophysical studies [*Torrence and Compo*, 1998; *Zhang et al.*, 2009]. *Thiebaut and Vennell* [2010] describe Hurricane Florence's impact on the Newfoundland coast and compare them to two other storms using wavelet and cross-wavelet analysis in a manner similar to the present study. Using wavelet analysis, they were able to identify the periodic motions excited by the passage of the storms and use it to determine the dispersion characteristics for the Newfoundland shelf. Similarly, the application of wavelet analysis to the LATEX current data and tidal data described above is likewise used here to identify the periodic motions excited on the Texas-Louisiana shelf by Hurricane Andrew.

For this study, the wavelet software package available from Christopher Torrence and Gilbert Compo and described by *Torrence and Compo* [1998] was used to perform the wavelet transformations on both the current records and the tidal records. The wavelet software package can be found at http://paos.colorado.edu/research/wavelets/. Corrections to remove a bias found in the low frequencies were additionally applied

to the software as described by *Liu et al.* [2007].

2. Group Speed Estimation

The method used for determining the group speed of the wave packet consisted of locating the time of maximum alongshelf velocity and the time of maximum surface displacement as a proxy for time of arrival of the wave. The maximum values for currents and water levels were taken from the hourly 40HLP data for the best determination of time of arrival.

The distance needed to determine the traveling speed of a wave is more complex for the Texas-Louisiana Shelf than simply taking shoreline distance due to the varying width of the shelf, the curvature of the basin, and the angle of the storm track. To best suit the complications of the shelf, distance from the storm track to each mooring was decidedly chosen to be represented by an along-isobath distance. Along-isobath distance from the storm track was measured as the summed great circle distances of the bathymetric data points along each representative isobath using the haversine formula. The summation begins at the point where the storm track crosses a given isobath, to the mooring on the isobath. Using distance along bathymetric contours rather than line of sight distance between moorings is more representative of a path a wave trapped on the coast may follow. A long wave would not necessarily follow every coastline deviation, so the isobars have been smoothed before summation with a simple running mean filter.

Group speeds were then estimated from the time of arrival and distances from the storm track using a linear regression between time and distance. Regression required that the time be the dependent variable and distance the independent variable, since the measurement of time of arrival is variable, and the mooring remains in a fixed location. Alternatively, *Thiebaut and Vennell* [2010] uses the scale-average time-series

derived from the wavelet transform to determine the group speed of wave in a more efficient fashion. This method however gave contradicting information probably due to other phenomena on the shelf affecting the scale average and is not discussed further.

3. Dispersion

Brink and Chapman [1987] describe a computer program that determines the dispersion characteristics for a given shelf topography and stratification and presents a method for comparing the estimated group speed and frequency to predicted group speeds at frequencies available. The software numerically solves the inviscid equations of motion for free wave solutions of linearized coastal trapped waves. Iterations determine frequencies at each requested wavenumber using the inputs of a rough shelf profile and N^2 profile. Thus, the dispersion curve returned displays frequencies that are theoretically possible for a particular shelf-slope region under the conditions of a particular stratification profile. The rough shelf-slope profile was obtained by using the Google Earth measurement tool to determine distance from the coast while recording the depth along the points of measurement. The profile was taken from along the 92° W meridian which coincides with moorings 18, 19, and 11. Stratification profiles have been determined from a LATEX maintenance cruise about a month before the storm from which CTD casts were made [*DiMarco et al.*, 1997]. Casts were made at moorings 17 (10 m), 18 (20 m), and 19 (50 m) along the 92° W meridian. A smoothed N^2 profile was obtained from the cast at mooring 19 as the representative stratification.

4. Theory

The following approach to coastal trapped wave theory follows from the method outlined by *Brink* [1991]. Starting with the coordinates of a straight coastline that lies along the y-axis at $x = 0$, with positive x pointing offshore, and z vertically upwards, and a bottom profile $h(x)$ that only varies in the cross-shelf direction, coastal trapped wave theory evolves from the linearized equations of motion for a stratified ocean.

$$u_t - fv = -\frac{1}{\rho_0} p_x, \tag{1a}$$

$$v_t + fu = -\frac{1}{\rho_0} p_y, \tag{1b}$$

$$0 = -p_z - g\rho', \tag{1c}$$

$$u_x + v_y + w_z = 0, \tag{1d}$$

and

$$\rho'_t + w\bar{\rho}_z = 0, \tag{1e}$$

where p is the pressure perturbation, u, v, and w are respectively the x, y, and z velocity components, f the Coriolis parameter, g the gravitational acceleration of earth, and subscripts represent derivatives with respect to the subscript parameter. The density, ρ, is understood to be a series of perturbations added to a reference density ρ_0

$$\rho_0 + \bar{\rho}(z) + \rho'(x, y, z, t),$$

where $|\rho'| \ll \bar{\rho} \ll \rho_0$. System (1) can be reduced to the equation of conservation of potential vorticity in terms of pressure

$$p_{xxt} + p_{yyt} + \left(f^2 + \frac{\partial^2}{\partial t^2}\right)\left(\frac{p_{zt}}{N^2}\right)_z = 0, \tag{2}$$

where N is the buoyancy/Brunt-Väisälä frequency and,

$$N^2 = -\frac{g}{\rho_0}\bar{\rho}_z. \tag{3}$$

Paired with boundary conditions, the equation can be constrained to behave nicely at each boundary of the shelf waters (coast, surface, bottom, and open ocean) and ensuring that the solution is a wave trapped at the coast. For the required boundary conditions there should be:
no normal flow (perpendicular) through the coastline

$$p_{xt} + f p_y = 0 \quad \text{at} \quad x = 0, \tag{4a}$$

a free surface,

$$p_z + \frac{N^2}{g} p = 0 \quad \text{at} \quad z = 0, \tag{4b}$$

no flow through the seafloor

$$\left(f^2 + \frac{\partial^2}{\partial t^2}\right) \frac{p_{zt}}{N^2} + h_x \left(p_{xt} + f p_y\right) = 0 \quad \text{at} \quad z = -h\left(x\right) \tag{4c}$$

and the pressure should asymptote to zero out to open ocean,

$$p_x \to 0 \quad \text{as} \quad x \to \infty, \tag{4d}$$

a necessity for the wave to be trapped to the coast.

Equation (2), as previously stated, is the conservation of potential vorticity. In a more familiar form, the conservation of potential vorticity equation is

$$\frac{\mathrm{D}}{\mathrm{D}t}\left(\frac{\zeta + f}{h}\right) = 0 \tag{5}$$

where ζ, the relative vorticity, is the curl of the horizontal currents $\nabla \times \vec{u} = u_y - v_x$, f the Coriolis parameter is also called planetary vorticity, and h the depth of the

column of water. The numerator $(\zeta + f)$ is together known as absolute vorticity, while the whole fraction $(\zeta + f)/h$ is the potential vorticity. The potential vorticity, if conserved, remains constant meaning that if one element changes, the other elements must change to remain constant. Thus, for a coastal column of water where f is nearly constant, moving the column to shallower water (decreasing h) requires that the relative vorticity also decrease in order for the potential vorticity to remain constant. Since relative vorticity cannot change immediately, a restoring force is initiated to balance out the change in potential vorticity, resulting in a wave.

In Equation (2), $p_{xxt} + p_{yyt} = \frac{\partial}{\partial t}(p_{xx} + p_{yy}) \sim (\zeta/h)_t$ since from Eqs. (1), in a geostrophic sense, $v \propto p_x$ and $u \propto p_y$. The remaining terms of Eq. (2) are approximately equivalent to $(f/h)_t$. However in Eq. (5), the column of water is homogenous and barotropic, so with the addition of stratification, a more complex representation of changing vorticity is required than by simply using depth. Therefore, knowledge of the vertical change in pressure and vertical change in density $(p_z/N^2)_z$ replaces the h.

If it is assumed that the solution takes the form of an alongshore wave multiplied by a cross shelf structure,

$$p = p(x, z)e^{i(\omega t + ly)}, \tag{6}$$

then using Eq. (6), Eq. (2) becomes,

$$0 = p_{xx} - l^2 p + \left(f^2 - \omega^2\right)\left(\frac{p_{zt}}{N^2}\right)_z, \tag{7}$$

which is now an eigenvalue problem with eigenvalues ω.

Typically, to solve the vorticity boundary value problem, a few simplifications are made. The first assumes that a long-wave limit approximation can be made, where the alongshore scales are much larger than the cross-shelf scales. The second

is that the time scales involved are much less than the inertial time scale. This allows the problem to reduce to a separable eigenvalue/eigenfunction boundary value problem, which may be solved analytically depending on the boundary conditions. Other various assumptions may be made to simplify the problem, such as no surface divergence (i.e. the rigid lid approximation) which changes the free surface boundary condition.

The equations used in the Brink program model are more complex and don't rely on the above simplifications, requiring numerical methods for solving. The model formulation for the Matlab® version of the program are found in *Brink* [2006]. This method allows for a mean alongshore velocity, v_0, and adjusts the equations of motion and diffusion equations to include advection and geostrophic balance.

$$u_t + v_0 u_y - fv = -\frac{1}{\rho_0} p_x, \tag{8a}$$

$$v_t + uv_0 + v_o v_y + wv_0 + fu = -\frac{1}{\rho_0} p_y, \tag{8b}$$

$$0 = -p_z - g\rho_2, \tag{8c}$$

$$u_x + v_y + w_z = 0, \tag{8d}$$

and

$$\rho_{2t} + u\rho_{1x} + v_0\rho_{2y} + w\rho_{1z} = 0, \tag{8e}$$

where v_0 is the mean alongshore velocity. This time ρ is structured as $\rho_0 + \rho_1(x,z) + \rho_2(x,y,z,t)$ with ρ_1 being the density field that is in geostrophic balance with the mean alongshore velocity, and similar to the previous method, $\rho_2 \ll \rho_1 \ll \rho_0$. Again, if it is assumed that the solution has the form of Eq. (6), the equations of system (8) can be combined to get the vorticity equation again in terms of pressure, albeit more

complex than Eqs. (2) or (7).

$$
\begin{aligned}
0 &= \omega' p_{xx} - 2\omega' s p_{xz} + \frac{\omega'}{N^2}\left(ff' - \omega'^2\right) p_{zz} - \omega'\left(Q + s_z\right) p_x \\
&- \left[-\omega' s Q + \left(\omega' s\right)_x + \frac{ls}{f}\left(f^2 - \omega'^2\right) - \left(\frac{\omega'}{N^2}\right)_z \left(ff' - \omega'^2\right) - \left(\frac{\omega'}{N^2}\right)\left(sM^2\right)_z\right] p_z \\
&- \left[lfQ + \omega' l^2 + lfs_z\right] p,
\end{aligned}
\tag{9}
$$

where

$$
\begin{aligned}
\omega' &= \omega + lv_0, \\
N^2 &= \frac{g}{\rho_0}\rho_{1z}, \\
M^2 &= \frac{g}{\rho_0}\rho_{1x}, \\
s &= \frac{M^2}{N^2}, \\
f' &= f + v_{0x}, \\
Q &= \left(ff^* - \omega'^2\right)^{-1}\left[\left(ff^* - \omega'^2\right)_x - s\left(ff^* - \omega'^2\right)_z\right], \\
f^* &= f + v_{0x} - M^2\frac{s}{f}.
\end{aligned}
$$

However, if mean alongshore velocity is ignored for the LATEX shelf (i.e. $v_0 = 0$ and $\rho_1(x,z) \to \rho_1(z)$), then Equation (9) reduces back to Equation (7) since $\omega' \to \omega$, $f' \to f$, $\rho_{1z} = 0$ therefore $M^2 = 0$ and $s = 0$, $f^* \to f$, and $Q = 0$. Equation (7) is to be solved numerically with the same boundary conditions (4) via resonance iteration, which involves finding the resonant frequency ω for a given alongshore wavenumber l. Resonance is defined as when the integrated pressure squared is at a maximum for a frequency [*Brink and Chapman*, 1987],

$$
\int_0^\infty \int_{-h}^0 p^2 \,\mathrm{d}z\,\mathrm{d}x. \tag{10}
$$

Once resonance is found for frequencies ω at wavenumber l, then a dispersion curve

can be contructed showing free coastal trapped wave modes for the system of topography and stratification.

CHAPTER III

RESULTS AND DISCUSSION

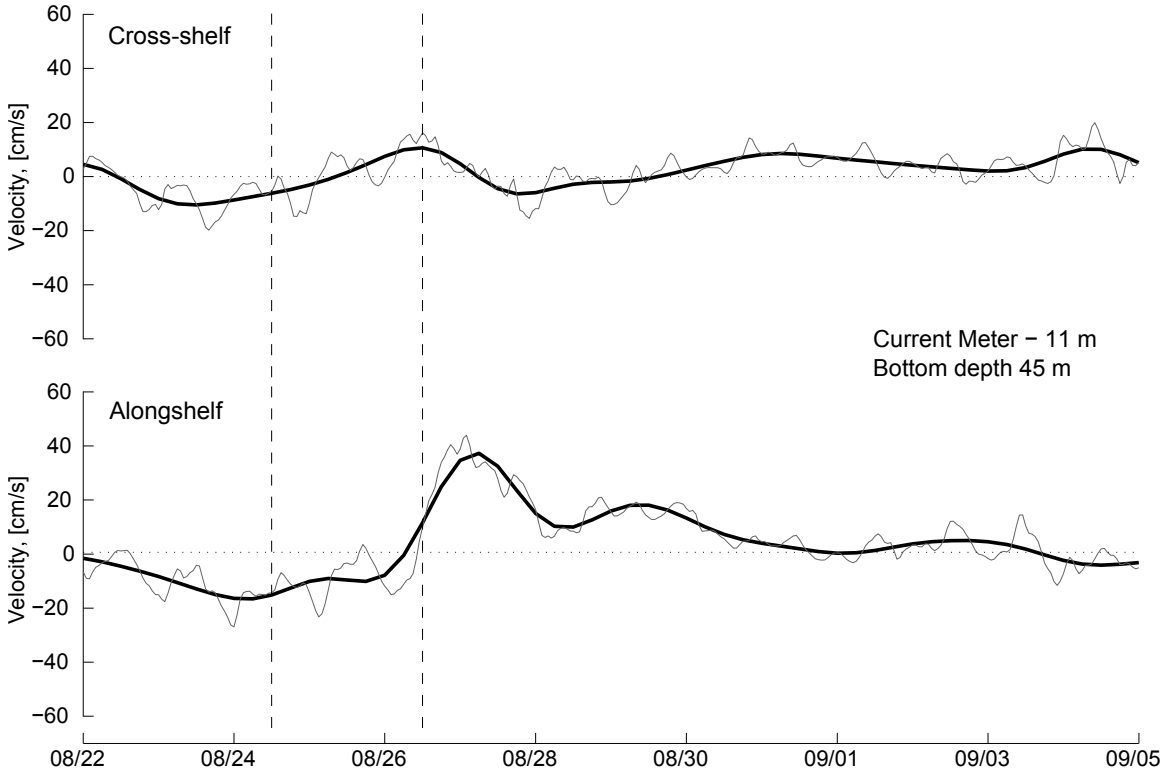

Fig. 3. Near surface currents from mooring 25 as a representative example of the strong alongshelf response to Hurricane Andrew. The thin line is the 3HLP currents and the thick line the 40HLP currents. The two dashed lines represent the time that Andrew entered and exited the Gulf and will be a common feature in all figures to represent the storm bounds.

A. Observed Currents

Following Hurricane Andrew's exit from the Gulf of Mexico, a current surge occurred in the alongshelf direction that exhibited maximum surface speeds of 130 cm/s near the storm track, and an average maximum surface speed of approximately

45 cm/s throughout the shelf. The typical response observed in most of the 40HLP surface currents west of the storm track is an initial small downcoast (negative) flow in the alongshelf component during the storm's presence followed by a strong upcoast surge after the storm's exit from the Gulf, resulting in a local maximum and leading to damped oscillations that persist for a few days. Figure 3 displays the 40HLP and 3HLP along and cross-shelf currents of the top instrument (11 m) at mooring 25, and demonstrates the characteristic alongshelf signal that is typical of most of the surface moorings to the west of the storm track.

The response of the 40HLP alongshelf currents is variable throughout the LATEX array, with the exception of a few stations on the 200 m isobath and those in the east nearest the storm. Figure 4 shows all of the alongshelf surface currents in relative positions revealing where the pattern exists and the variation between the moorings. The 3HLP currents are simultaneously included on the figure and show a large amount of inertial response (local inertial is very close to diurnal) confined to the easternmost moorings. The inertial response to the easternmost moorings give an estimate on the limits of the direct forced effect of the storm and imply that the remaining shelf is allowed to propagate freely [*Brooks*, 1983].

The remainder of the analysis focuses its efforts on the alongshelf currents of the 40HLP data due to the subinertial nature and majority of variability of a coastal trapped wave primarily occurring in the alongshelf direction, particularly in the long wave limit where the alongshelf scales are much greater than the cross-shelf scales [*Brink*, 1991]. Here after, currents and velocity are understood to be the 40HLP alongshelf current components of the surface most instruments unless otherwise noted.

Using the difference between the minimum and the maximum velocity as a simplistic metric for the response size, it becomes apparent that a cross-shelf structure exists with the largest amplitude in the middle of the shelf. The largest responses

occur along the 20m isobath with an average difference of 60 cm/s. The next largest responses occur over the 50 m isobath with an average of 40 cm/s difference, and a single surface observation of 45 cm/s difference on the 10 m isobath. The response on the 200 m isobath line is nearly absent or greatly diminished, but the few moorings that still exhibit the signal's pattern (the farthest from the storm) have an average difference of about 15 cm/s.

There is a substantial time lag between the times of maximum velocity that increases away from the storm track as seen in Figures 4 and 5. Figure 5 particularly demonstrates the lags in time of maximum velocity at distance from the storm track on the 20 and 50 m isobaths. The 200 m isobath shows a diminished response by a lack of any apparent pattern of propagation, or at least not as clear of a propagation of the signal as the 20 and 50 m isobaths. The successive time lags suggest a propagation of the signal in the downcoast direction, in the Kelvin wave sense. The time difference between moorings near the storm to the westernmost moorings is about a day and a half, suggesting a group speed of about 500 km/day or 6 m/s.

The diminished response at the shelf break could be attributed to the rough topography of the slope and shelf break, or in part to an anti-cyclonic eddy system sitting in deep water past the slope off shore from mooring 12 (approx. 25.5°N 90°W) at the time the storm came through [*S.A.I.C.*, 1994]. The most likely explanation is that the response terminates near or has significantly decayed before reaching the shelf break. Figure 4 illustrates the strength of the signal on the inner shelf, and the absence or weaker response over the shelf break suggesting that the response has a cross-shelf modal structure with an amplitude that is largest over the mid-shelf

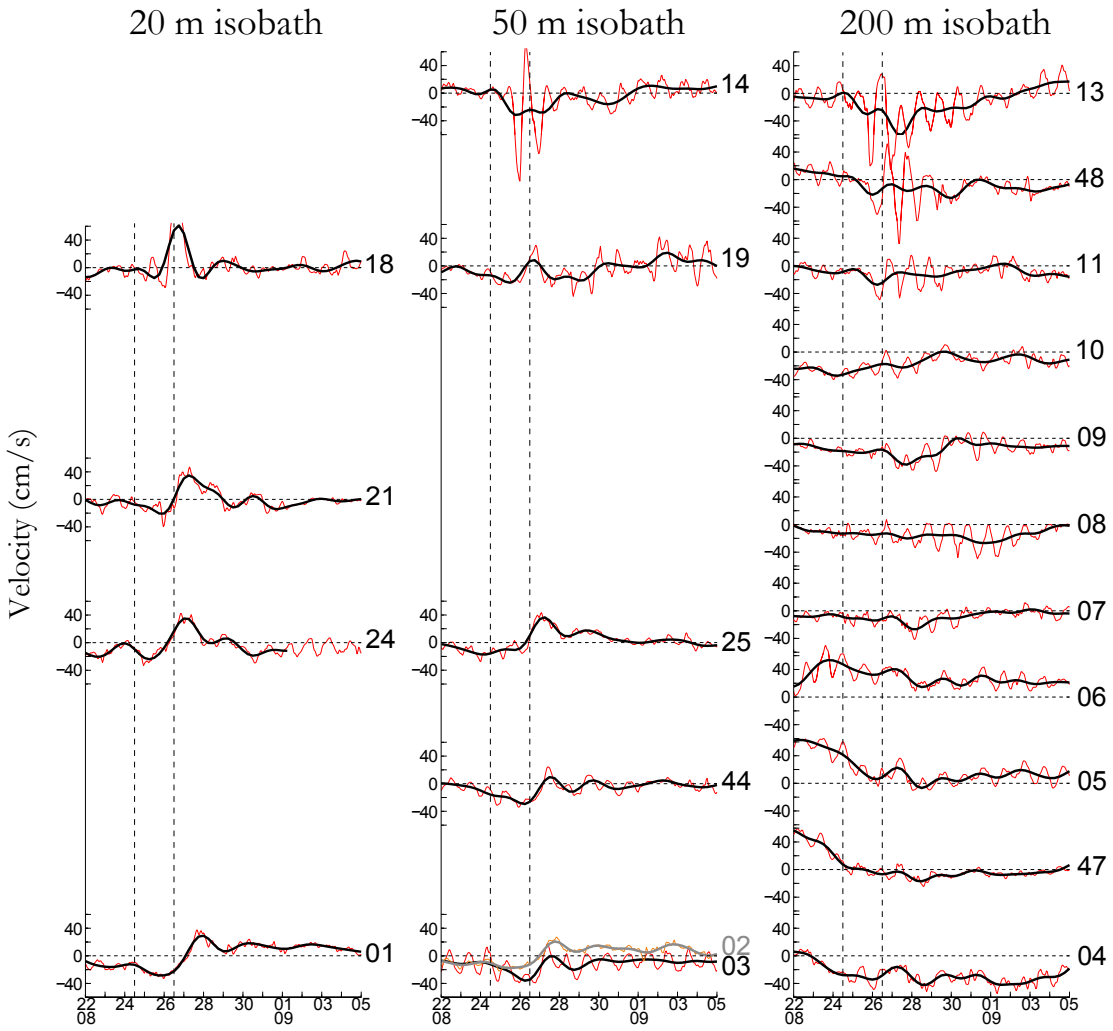

Fig. 4. The alongshelf currents positioned in a manner representing their relative positions on the shelf (in linear distance from the storm track). The black lines are 40HLP velocities and the red lines are 3HLP velocities (without tides removed). Easternmost moorings are at the top, and down the figure progresses westward, then southwest through the bend

and decays towards the shelf break where it either reaches a nodal point, or continues decay towards the open ocean, depending on the modes activated [*Brink*, 1991]. The signal features a measurable amount in the currents at the inshore-most moorings, and as shown in the next section exhibits a surface displacement at the coast.

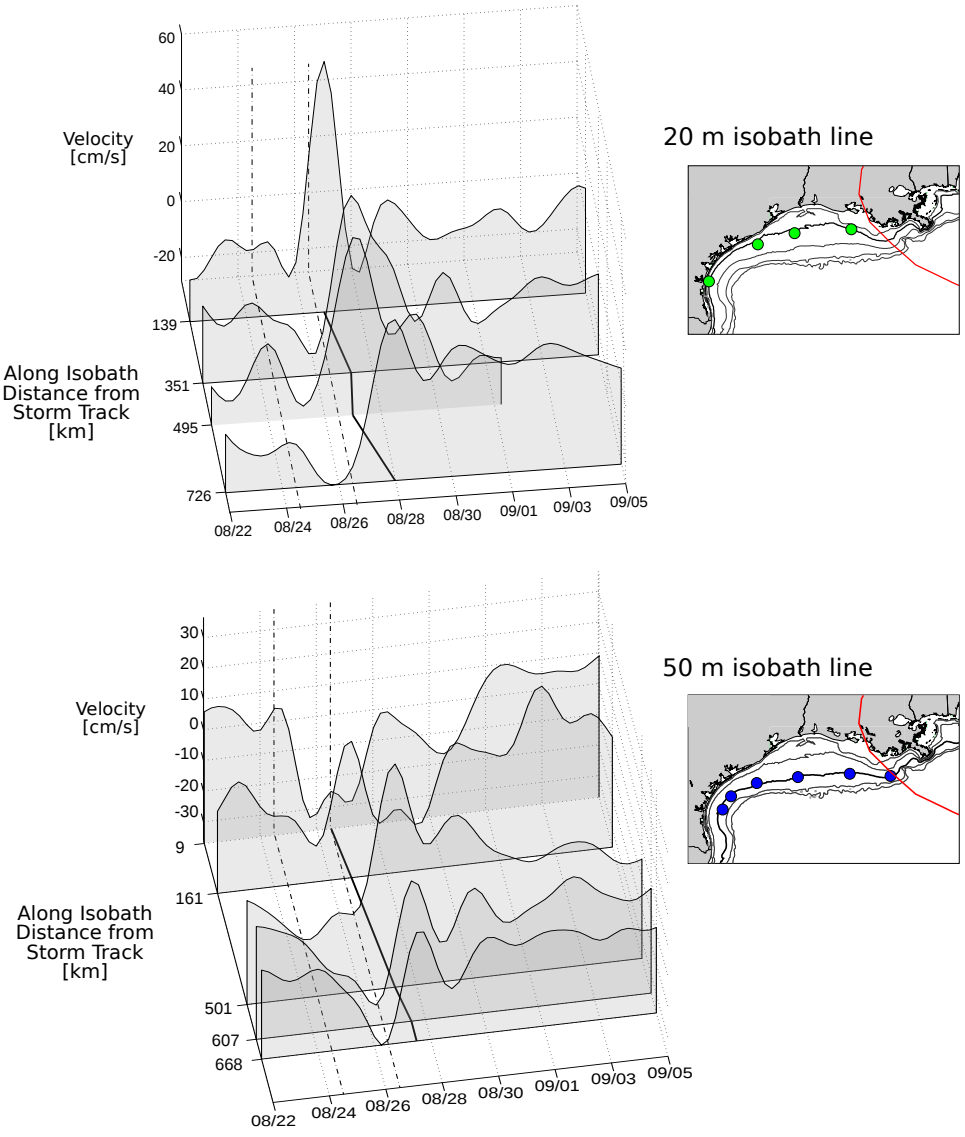

Fig. 5. Time lags in the alongshelf surface currents on the 20 m and 50 m isobaths. The map inset shows the locations of each mooring. The dashed lines represent the storm's entry and exit of the Gulf of Mexico, and the thick line at the bottom of the figure represents the projection of the max current onto the distance vs time plane.

B. Observed Surface Elevations

The residual tidal records display a pattern similar to that of the surface currents, only inverted (Figure 6). During the storm's presence, each station features a small initial peak, on the order of 0.2 m followed by a larger trough structure with its largest amplitude at 0.5 m. Time lags are also observed in the maximum surface displacement of the trough, increasing in the stations farther from the storm track suggesting a propagation in the downcoast direction. The small peak initially is sharp in the records closest to the storm track and spreads out in the records farther away from the storm track, but does not appear to have a time lag, as its maximum is approximately at the same time throughout the records. The trough has it's largest amplitude of 0.5 m in the Sabine Pass record, nearest the storm track, and has diminished to about 0.1 m by the time the signal reaches Port Isabel, the farthest station from the storm track and southernmost station of either observation type. Though the signal had diminished by the time it reached Port Isabel, it was still identifiable and implies continued propagation farther into the Mexican shelf system. The time differences from the Sabine Pass station to the Port Isabel station is about a day which approximates to a propagation of about 550 km/day or about 6.5 m/s; a very good agreement with the propagation estimate from the currents. A more thorough estimation of propagation speed is given in a later section using a regression analysis.

The small peak and trough structures in the tide guage data agree well with the patterns found in the currents. An ideal propagating plane wave is predicted to have currents beneath the wave crest that flow in the same direction as the propagation, and currents beneath a trough should exhibit flow in the opposite direction of the wave propagation as described by *Gill* [1982]. For a westward/downcoast propagating

trough, the currents would be expected to flow towards the eastern/upcoast direction, which is what is observed here. The small peak in water levels corresponds well with the initial downcoast flow of the currents, and the trough with the strong upcoast surge.

C. Wavelet Results: Evolution of the Low-frequency Spectrum

Wavelet transforms were performed on most of the alongshelf and cross-shelf records of both the 40HLP and 3HLP, excluding only records without continuous data throughout the time range of the storm event and the several weeks following. The exclusions are part of the necessity that the transform, due to its filtering nature, is less reliable near the terminating ends of the data record, nor in proximity to points where data gaps occur. The focus remains on the alongshelf currents as there were no immediately discernible patterns found in the cross-shelf wavelet transforms. Common to most of the alongshelf wavelet transforms is a signal immediately following the storm's exit in the 2–4 day period range, and is seen in both the 40HLP and 3HLP datasets. Figure 7 shows the typical wavelet transform from the top instrument of mooring 03, displaying the characteristic 2–4 day signal and Figure 8 shows all of the wavelet transforms of the surface alongshelf currents. Many of the transforms show energy with greater than 95% significance (black contours) in periods of 8 days and longer. Peak energies within these periods occur inconsistently throughout the shelf, so it is ambiguous whether or not these periods are related to coastal trapped waves, activated as a result of the storm, red noise that arises from stochastic phenomena such as wind driven currents, or other long period events.

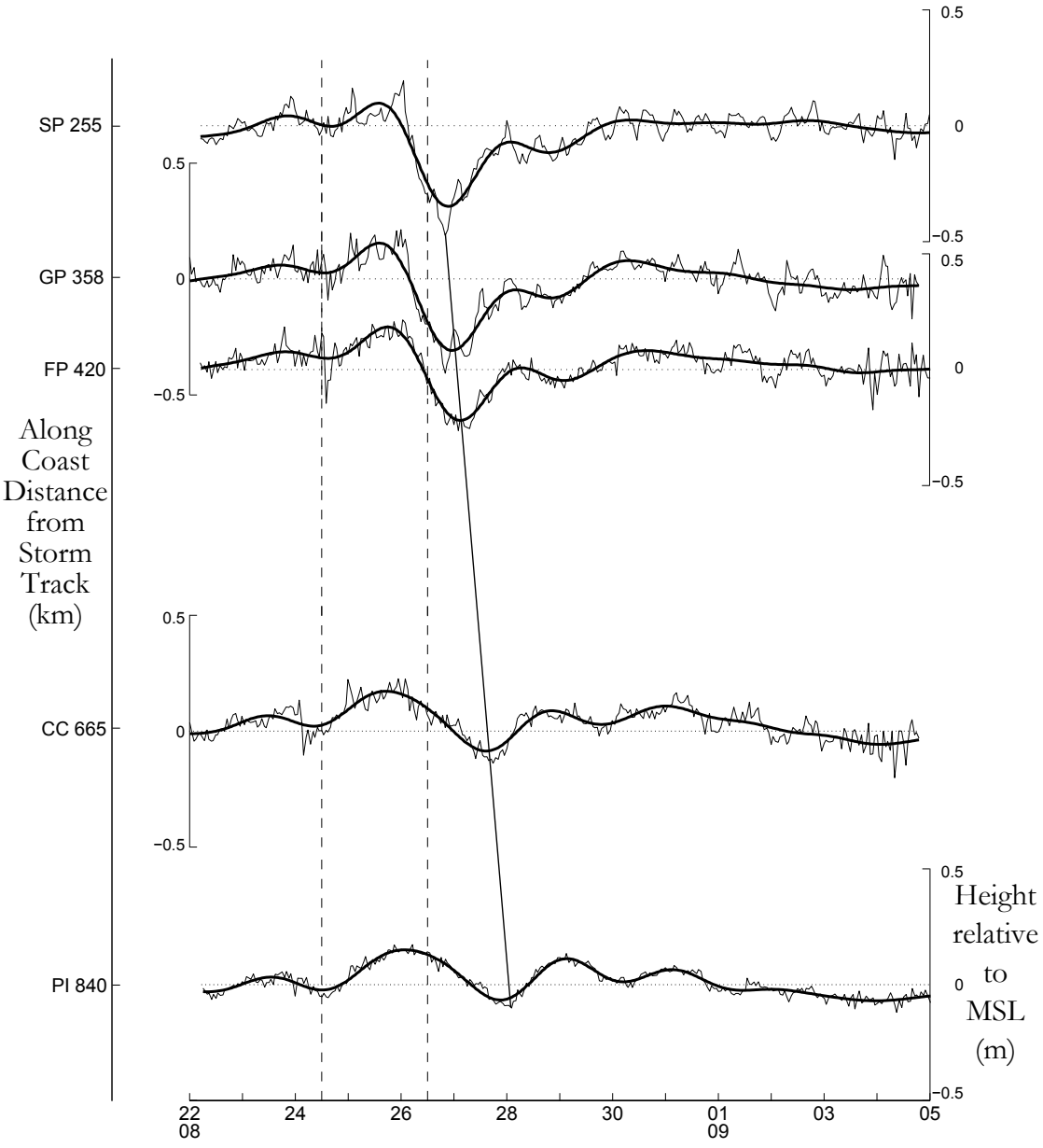

Fig. 6. Residual surface elevations positioned in their relative spatial positions along the coastline. The thicker black lines are 40HLP data and the thin lines are unfiltered residual surface elevations. The diagonal line is drawn to show the approximate time lags and propagation of the signal

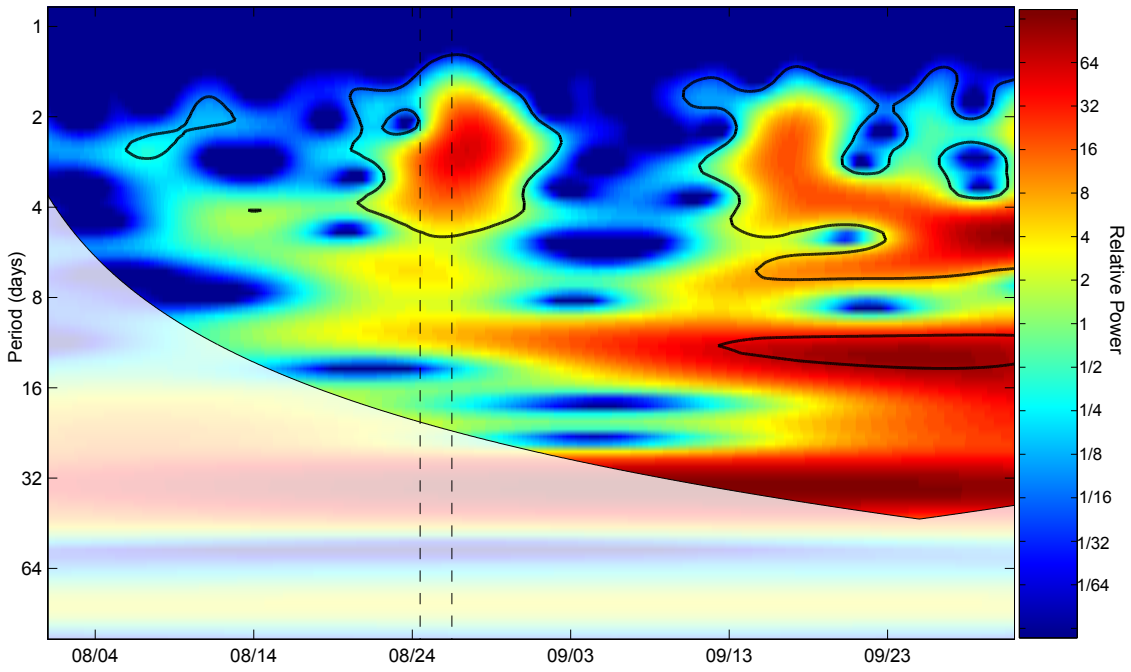

Fig. 7. Representative wavelet transform from mooring 03 showing a prominent peak in wavelet power at 2–4 day periods following the passage of the storm. The colors are based on relative power with red being the greatest power and blue being the least power. The black contour lines are the 5% significance levels.

The wavelet transforms, when arranged spatially similar to the mooring arrangement on the shelf (Figure 8), display a pattern of greatest power in the moorings nearest the storm track, while the moorings farthest from the storm have less power, but still feature a prominent signal. As previously noted in the spatial plots of alongshelf currents, the largest response of power in the 2–4 day signal occurs in the 20 m isobath moorings, a strong but diminished signal is seen in the 50 m isobath moorings, and a weak, though apparent, signal displays in the 200 m isobath moorings. The decay of the signal towards the open sea reinforces the suggestion of a trapped wave response with its largest amplitude over the middle of the shelf that either asymptotes to sea level beyond the shelf break or a nodal point exists near the shelf break. Some

records (particularly the farthest on the 200 m isobath line) exhibit energy in the 2–4 day period range previous to the occurrence of the storm that has nearly equal or greater power than that following the storm. This may be due to the aforementioned eddy present just off the slope producing some variance in the same period range; otherwise, the energy of the storm response may have a large enough signal relative to other phenomena in that period band.

The LATEX moorings occupy the region of latitude between 27 and 30 degrees North. Within this region, the inertial period, determined by $T_i = 2\pi/f$, ranges from 1.00 days at 30° N to 1.14 days at 27° N. A 2–4 day signal is then sufficiently described as a sub-inertial signal which is consistent with lower frequency coastal trapped waves.

Wavelet transformations were additionally performed on the residual water levels from the tidal records. In agreement with the transforms of the current records, there exists a 2–4 day signal that occurs just following the storm's exit. The signal is strongest in the Sabine Pass record and decays slightly over the distance to Port Isabel, the final station before Mexican waters. Figure 9 shows the wavelet transformation of all of the tidal stations arranged spatially in order.

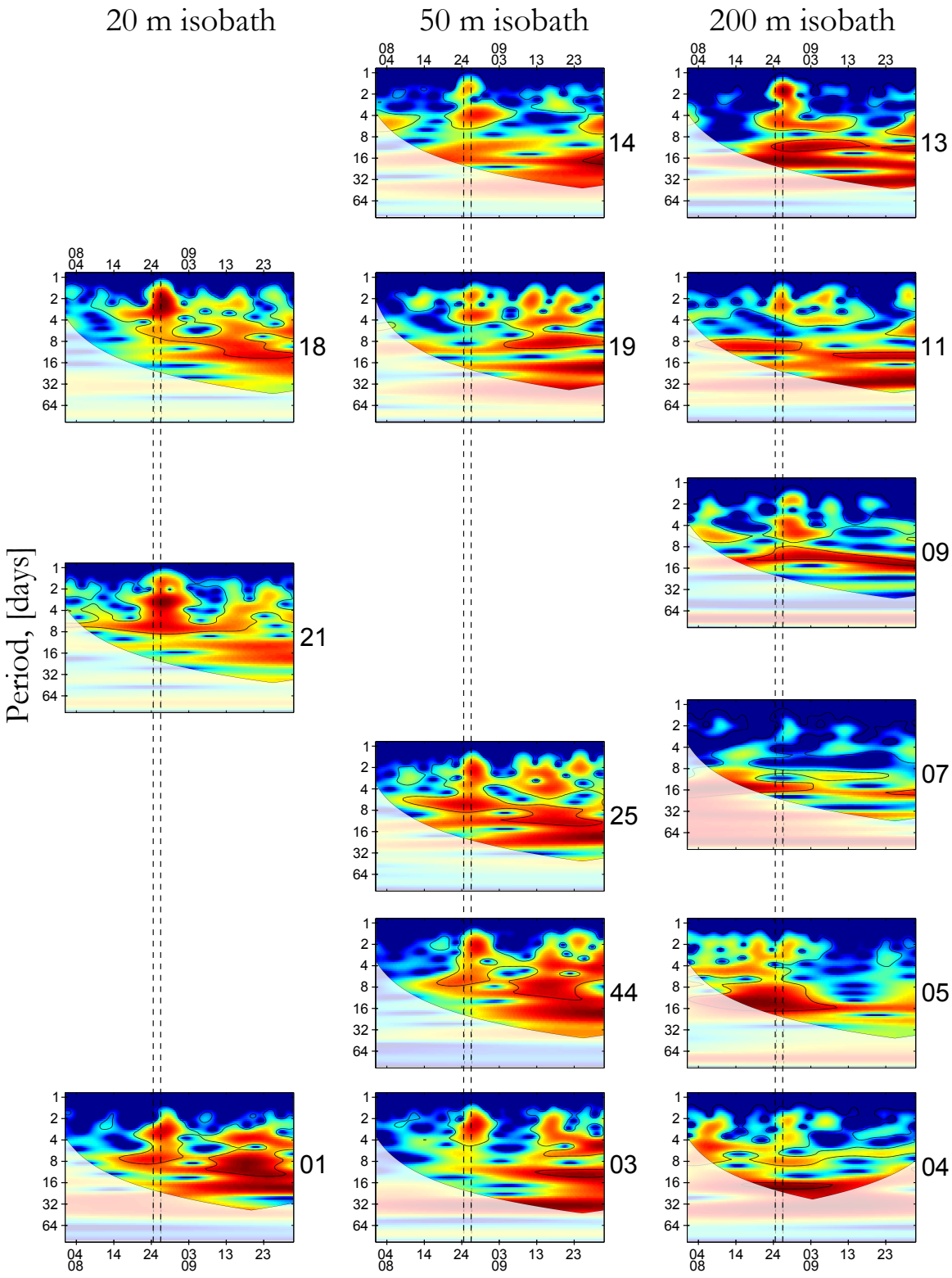

Fig. 8. Alongshelf current wavelet transforms in their relative shelf positions. The same positioning as Fig. 4 is used, and the same colorscale as Fig. 7.

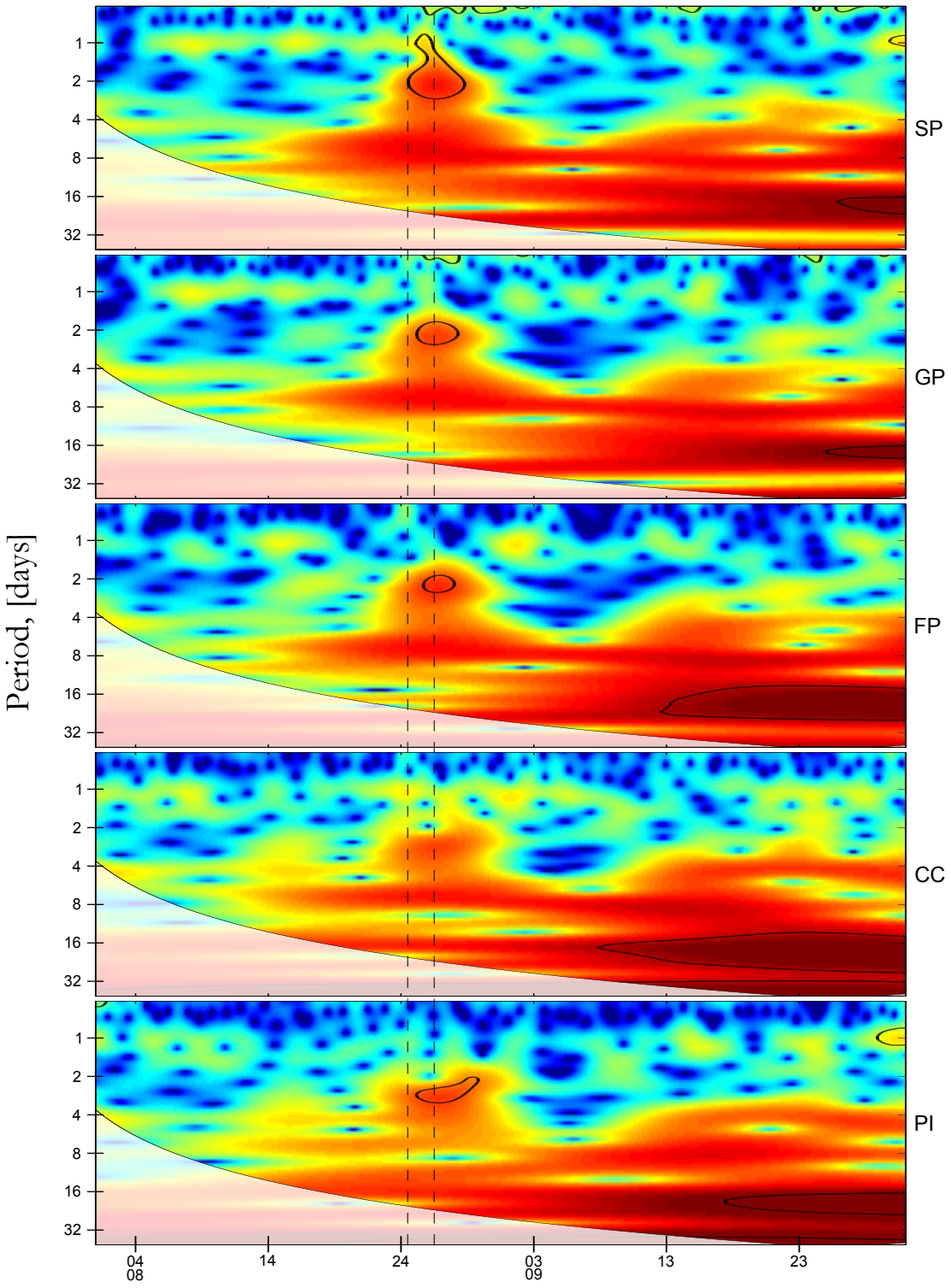

Fig. 9. Residual surface elevation wavelet transforms. The same positioning as Fig. 6 is used, and same colorscale as Fig. 7.

D. Estimation of Group Speed

Propagation of the post-Andrew signal has now been established along the coast in both the maximum currents and in the surface displacement of sea levels. Furthermore, activation of subinertial energies in 2–4 day periods are found to be common to both sea levels and currents, providing a convincing case of a coastal trapped wave. The next step in characterizing the wave is to make a determination or estimation of the group speed. This was done by using all estimates of the time of peak values at each station including the top, middle, and bottom current meters where available, and each tidal station in a regression of time with respect to distance from the storm track. Regression requires that time be the dependent variable and distance the independent variable, because the measurement of the time of peak value is variable, and the moorings were in fixed locations. The units of the regression line slope is the inverse of speed (s/m), which is used to estimate group speed. *Thiebaut and Vennell* [2010] used a scale averaged time series derived from the wavelet transform to determine the group speed of a wave in a more efficient fashion, and initially was planned to be used in this study. However, this method was not ultimately used as it gave contradicting information probably due to other phenomena on the shelf affecting the scale average.

Figure 10 shows the least squares fit regression line based on the pooled time estimations from each measurement along with the 95% confidence levels with an R-squared value of 0.72 and a p-value of 2.02×10^{-11}. The slope estimate, 6.73 m/s, is the inverse of the slope shown, since it is in units of time per distance. The 95% confidence values then give bounding speeds of 5.55 m/s and 8.54 m/s. A speed of approximately 6.7 m/s agrees nicely with the initial simplistic estimation in Chapter II, and is close to speeds that have been observed in other coastal trapped wave

analyses (Table I). Each category of data points (20 m isobath, tide stations, etc.) were also individually submitted to a least squares regression analysis, which closely agreed with pooled data.

Table I. Similar observed propagation speeds.

Date	Speed (m/s)	Location	Reference
1962	5	SE Australia	*Hamon* [1962]
1984	4.6–6.9	W Australia	*Fandry et al.* [1984]
1997	5	NW Australia	*Tang et al.* [1997]
1992	6.73	NW Gulf of Mexico	This study

An interesting general feature of the regression Figure 10 is that the points from the 200 m isobath tend to be beneath the regression line, and the points from each successive inshore isobath line up to the tide stations tend to be above the regression line. The level ordering of the points is probably due to either the choice of origin of the distance measurements (the angled storm track) or the translation of the hurricane at successive times over each isobath. Changing the mooring distances relative to the 91° W meridian, however, does not affect a large change, and the leveling structure still appears. The levels suggests successive generation times for the signal and, using the intercepts and the known times and locations of the storm, the storms location when the wave was generated can be shown.

Since the regression analysis was additionally run independently for each isobath and tidal stations and the intercepts are time values, then using those intercepts, the 95% confidence intervals, and the storm track as a time line, a generation region of the propagating signal can be estimated. The time of each intercept value was plotted along the times of the storm track along with the confidence bounds for each isobath

category which traces the wave back to the time it was generated along the storm track. This provides a rough estimation for when the wave was generated in relation

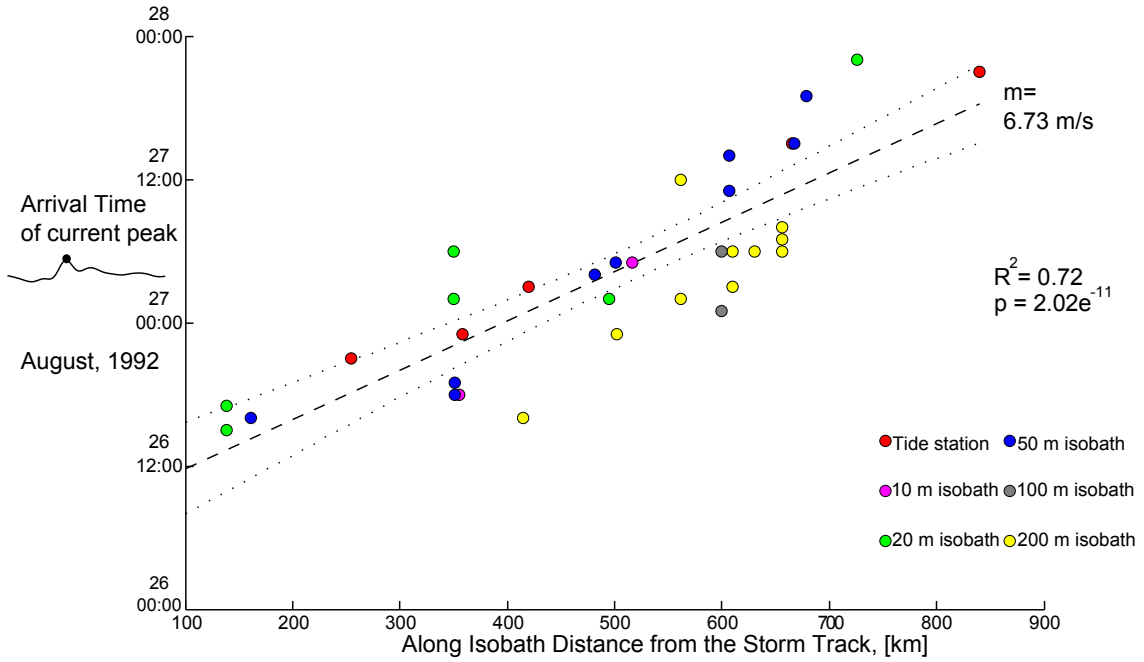

Fig. 10. Group speed estimation using regression of the combined times of arrival of the wave. The dashed lines are the 95% confidence intervals of group speed. The points are color coded for water depth, as in Fig. 2

to the hurricane's position. While no clearly definitive time can be established for when the wave began propagating, the results are consistent with a generation time that coincides with the time the storm made landfall and exited the Gulf. Unfortunately, no statement can be made as to whether the relaxation of pressure is the release moment for the wave to begin propagating, or whether it is wind shear, or relaxation of the trailing storm winds. Figure 11 shows the plotted intercept values and confidence bands along the storm track.

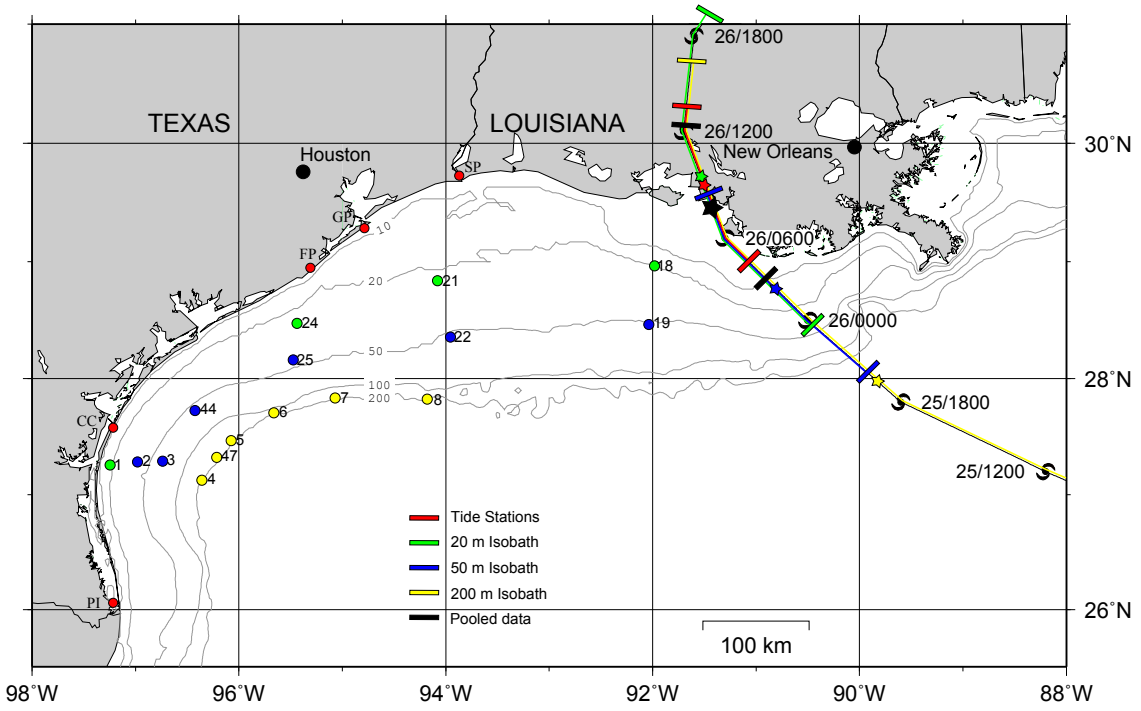

Fig. 11. Estimated generation region as determined from the intercepts of group speed estimation regression. The stars are the estimated time and position of generation along the storm track, and the bars are the 95% confidence intervals. The colors again represent the isobath categories.

E. Dispersion Relation

Using a bathymetry profile from the shelf and slope along the the 92° W meridian and a N^2 profile taken from the 50 m isobath as inputs to the coastal trapped wave solving program [*Brink and Chapman*, 1987], a dispersion curve was created representative of the eastern LATEX region (Figure 12). The trapped wave program requires and initial frequency guess; using an initial guess of a 2 day period returned the first coastal trapped wave mode (i.e. pressure crosses the $z = 0$ line once). Further inputting a range of frequencies returned the second and third coastal trapped wave modes and a Kelvin wave mode in the lowest frequencies. In Figure 12, the red

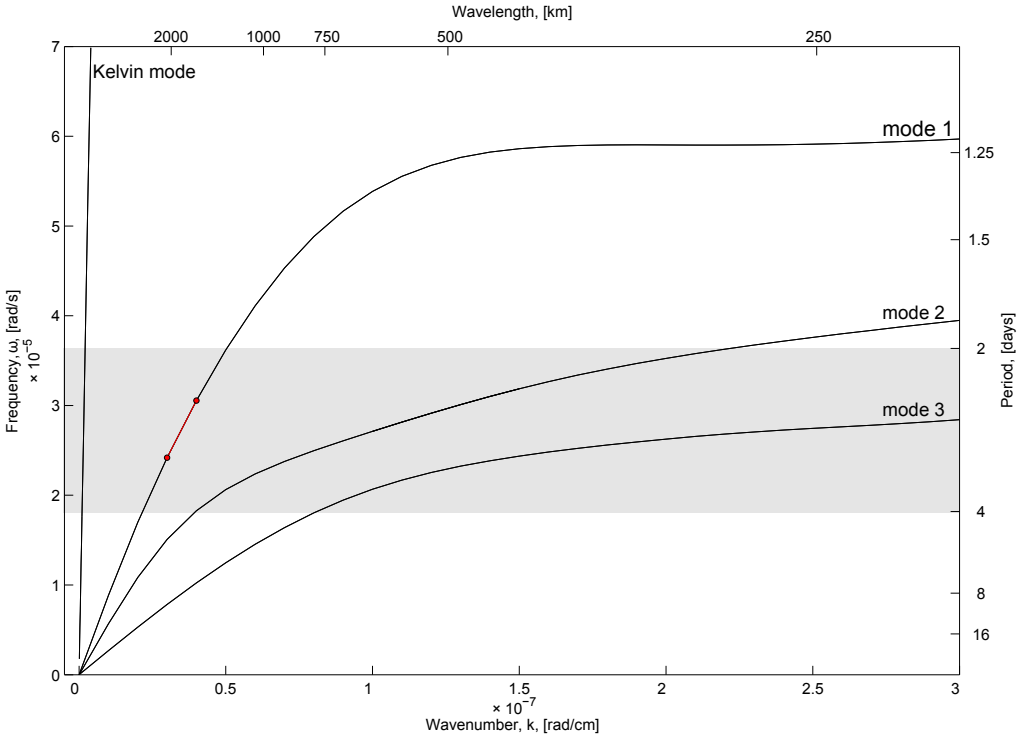

Fig. 12. Dispersion curves for the first three coastal trapped wave modes and Kelvin mode on the TX-LA shelf at 92° W. The band of gray highlights the region of 2–4 day periods noted from the wavelet analysis.

highlighted points along the first continental shelf mode correspond to periods of 2.4 days and 3.0 days, along with phase speeds (ω/k) of 7.6 m/s and 8.1 m/s. Group speed is simply the slope of the line, $\mathrm{d}\omega/\mathrm{d}k$, providing a theoretical group speed of 6.36 m/s along the red line, which agrees well with the observed group speed of 6.73 m/s and is found in the observed range of 2–4 day periods. According to the dispersion curve, the wavelength that corresponds to this group speed is between 1571–2094 km. The other modes produce group speeds slower than the observed speeds. Interestingly, 4 and 8 day periods are observed for the second and third modes for the same wavelength range given by the first mode, which in the wavelet transforms are another common period observed for the time records, though it was

ambiguous as to when these periods where activated or reached peak energies (Figures 8 and 9).

Figure 13 shows the calculated cross-shelf structure of pressure and along-shelf velocity of the first mode from the coastal trapped wave program. The calculated cross-shelf structure is very similar to what was observed in the cross-shelf structure of the alongshelf currents on the shelf (Figure 4); a large inshore amplitude that decays offshore. Additionally, the calculated velocities of ~ 40 cm/s, and pressure of $3 \times 10^{-}1$ dbar (roughly 30 cm) are similar in magnitude to what was observed in the alongshelf currents and residual water levels.

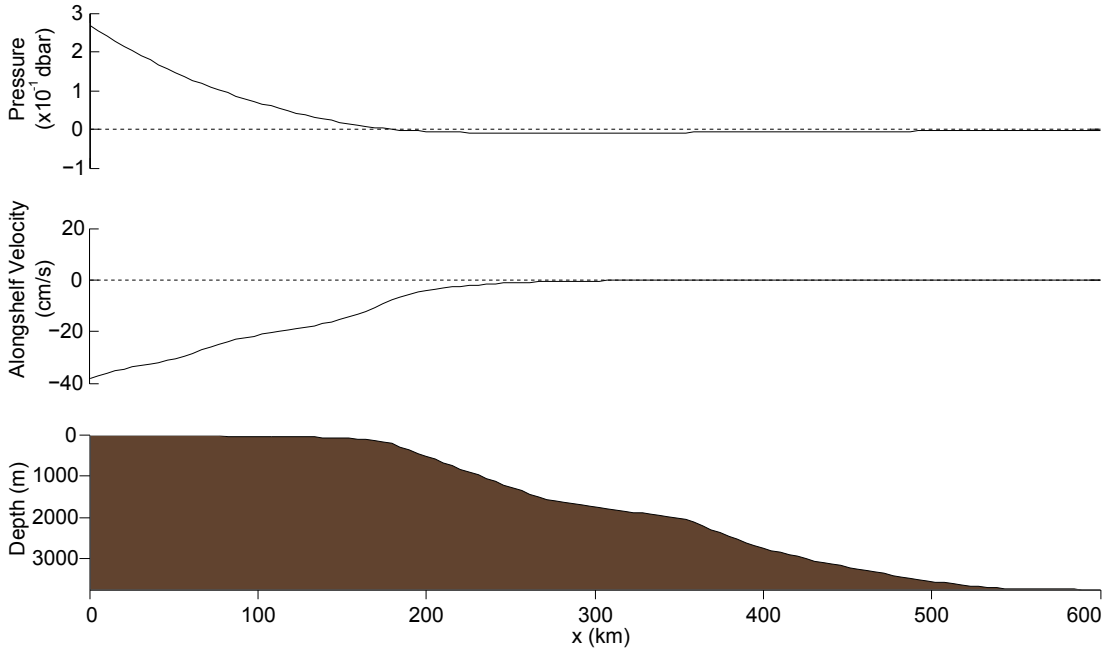

Fig. 13. Cross-shelf structure of pressure and alongshelf velocity for the first mode as output from the coastal trapped wave program.

Brink [1982] describes a diagnostic that is a useful characterization of the dominant restoring force for a freely propagating coastal trapped wave mode; $R = K/P$,

where K and P are the shelf integrated energy states, kinetic energy ($\propto \vec{v}$) and potential energy ($\propto \partial p/\partial t$ due to isopycnal perturbations including the surface). If $K \gg P$, $R \gg 1$, then there is greater current motion than surface or isopleth displacement, and potential vorticity dominates as the wave's restoring force; meaning the wave is more barotropic and shelf wave-like. Indeed, in the barotropic limit with the rigid lid assumption and sloping topography, R becomes infinite. Oppositely, when $K = P$ (the energy is equally partitioned), $R = 1$, the dominant restoring force is gravity; meaning it is more Kelvin wave-like. In the case of a flat bottom, the case where Kelvin waves exist, the potential vorticity can no longer change with depth, so changes in pressure create kinetic motions and the motions are restored by gravity.

In addition to calculating the dispersion curves and eigenfunctions (modal structures) of the free coastal trapped waves, Brink's Program also calculates the kinetic and potential energies for each mode. Mode 1 for the cross-shelf line at 92° West has $R = 17.24$, meaning that the wave mode consists of more current flow than surface disturbance and features more of a barotropic shelf wave-like response. Figure 14 corroborates the barotropic character since over the majority of the shelf the currents at each depth level are nearly in unison. When the response is barotropic, the entire water column flows at the same velocity and has no change with depth. Figure 14 demonstrates that the shelf exhibited currents that are mostly barotropic, particularly in the western region. Though some are incomplete, the moorings nearest the storm track exhibit some baroclinic characteristics as seen in the variable response in velocity at different depth levels. This is to be somewhat expected since the area nearest the Mississippi River has much greater freshwater input leading to stronger stratification and would be expected to have a stronger baroclinic component.

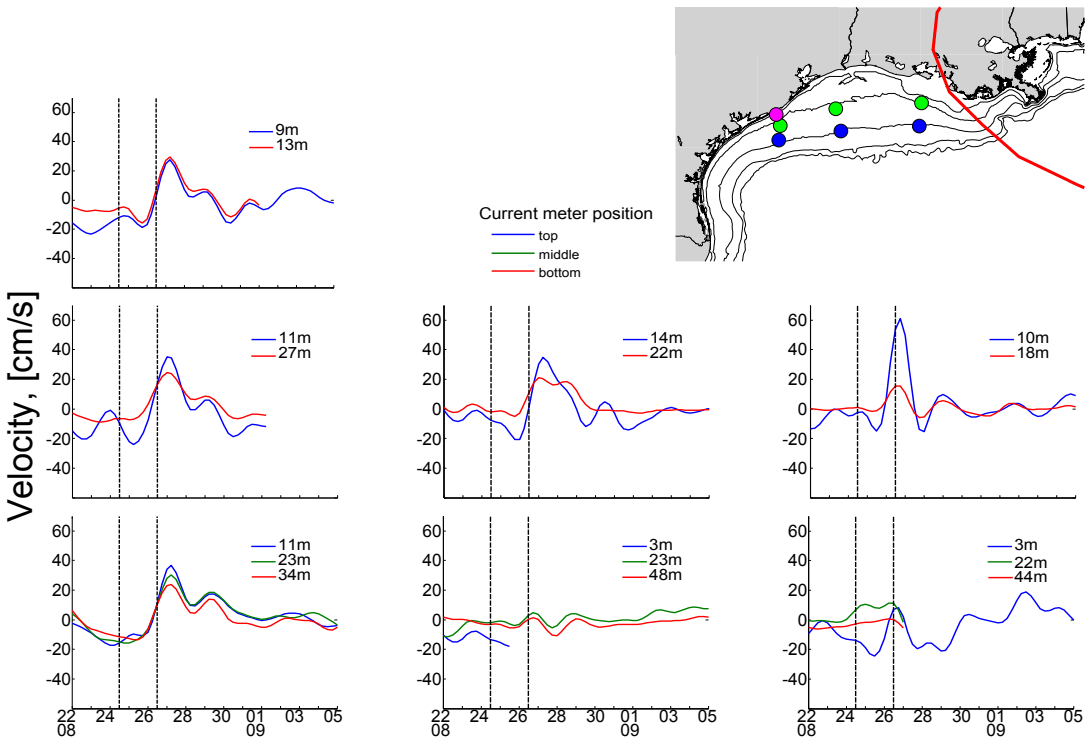

Fig. 14. Vertical levels of currents showing the dominant barotropic signature. The subplots are in the same relative positions on the shelf as shown on the inset map.

CHAPTER IV

CONCLUSION

Following the passage of Hurricane Andrew across the LATEX shelf, the propagation of a wave along the coast from the Mississippi river delta to the Texas/Mexico border has been observed in both the sea surface and in the alongshelf currents. Prominent frequencies were discovered, a group speed was estimated, and dispersion curves calculated for the area, all which point to the occurrence of a coastal trapped wave. The structure of the observed alongshelf currents reflect that of a coastal trapped wave *Mysak* [1980]; *Brink* [1991]; *Tang et al.* [1997] for several reasons. First, the wave was confined to the coast. The observations show that the greatest amplitude occurs inshore at the 20 meter isobath moorings, and decays offshore with a minimum near the shelf break as seen in the 200 meter isobath moorings. The amplitude of the signal is seen to have a time lag in the alongshelf currents that describe a downcoast (parallel to the coast) propagation. Tidal gauge data also shows the existence of a half meter trough surface displacement that travels down the coast. Less than a meter surface displacements are similar to the findings and model of *Tang et al.* [1997]. The modeled first coastal trapped wave mode demonstrates the same cross-shelf structure, that pressure (i.e. surface displacement) and the alongshelf currents feature their largest amplitude inshore and decays offshore to sea level for displacement (to zero for pressure difference), and to zero for alongshelf flow.

A description of a coastal trapped wave, provides a good possible explanation for the weakly observed signal and propagation along the 200 m isobath. It is likely that either the cross-shelf structure has sufficiently decayed by the shelf break on the wide LATEX shelf, or that a node in the modal structure occurs near the break. It is also possible that propagation does not show up as clearly due to the rough

topography of the shelf break and slope in the northwestern Gulf of Mexico, as *Brink* [1980] demonstrates that irregular bottom topography can induce damping due to scattering and phase velocity changes.

Wavelet transforms of water levels and currents on the shelf show that the dominant frequencies following the storm are subinertial (i.e $\omega < f$), which is typical of long wavelength coastal trapped waves. Periods in the 2–4 day range are the prominent periods of the wavelet transforms for both currents and water levels. Viewing 2–4 day periods on the modeled dispersion curve shows that a predicted group speed is quite close to that speed that is observed. A group speed of 6.35 m/s is predicted from the model program [*Brink and Chapman*, 1987; *Brink*, 2006] for the 2–4 day period range for the first mode coastal trapped wave on the Texas Shelf, and an estimated group speed of 6.7 m/s is actually observed from the combined current and the sea level observations.

The calculated energies of the first mode from the model reveal that the kinetic energy is an order of magnitude greater than the potential energy, meaning there should be greater vorticity than surface or isopycnal oscillation. Though the water column over the shelf had a stratified structure, the model still predicted that the wave should have greater characteristics of a voriticity shelf wave, than an internal Kelvin wave. *Tang and Grimshaw* [1995] predicted that the response to a tropical storm was dominated by low-mode barotropic shelf waves, and *Tang et al.* [1997] confirmed this with a model and observations to Tropical Cyclone Jane. The observed alongshelf currents are as predicted, largely barotropic and shelf wave-like, though there is likely a small baroclinic component (especially near the storm track) making the wave a slight hybrid trapped wave.

Many studies have linked the generation of shelf waves to the alongshelf wind stress [*Adams and Buchwald*, 1969; *Gill and Schumann*, 1974], so it is of interest to

try to determine the generation mechanism from Hurricane Andrew that leads to the free wave response on the rest of the shelf. The estimation of group speed establishes an estimated generation time from the intercept of the least squares line and can be used to estimate the storm's position at the time of the generation of the wave. The generation time coincides with the progression of the tail end of the storm onto land as expected, close to the time the eye moves on shore plus or minus a few hours. The hourly time step creates an uncertainty of whether or not the generation mechanism of the shelf wave is the release of the storm surge, or the tail end of the wind stress.

KG99 mention two possibilities as generation mechanisms of the trapped wave generated by Hurricane Andrew. Upwelling caused by the tail end wind stress, or relaxation of the storm surge could possibly have resulted in a change in potential vorticity and generated the shelf wave. KG99 describe the observation as a barotropic Kelvin wave and an internal Kelvin wave resulting from the relaxation of the storm surge in the moorings that they studied, and note that the speed should be 14 m/s for an average shelf depth of 20 m. However, on the western shelf in the region free from the direct forcing of the hurricane, only a shelf wave response was observed; no evidence of a Kelvin-like wave was found. As calculated by the coastal trapped wave program, the Kelvin wave speed should be approximately 179 m/s, much faster than the observed speeds of 6.7 m/s. The predicted speed of a barotropic Kelvin wave, $\sqrt{gH}$, where H should be the deepest depth and not the average bottom depth [*Brink*, personal communication], is 171 m/s for 3000 m depth, very close to the speed from the program. *Mysak* [1980] describes H as being something like the depth that the Kelvin wave "feels" which leaves room for interpretation as to which depth is "felt", whether it is the deepest depth possible, or the average depth of the shelf. Viewing Figure 12, the Kelvin wave mode is shown to occur only in the very large wavelengths; this is also the case in dispersion curves found in other studies [*Cutchin and Smith*,

1973; *Mysak*, 1980]. The average shelf depth of the LATEX shelf is say 50 meters which using $\sqrt{gH}$ would produce Kelvin speeds of 22 m/s. Even an average depth of 20 meters gives 14 m/s, still larger than the 6.7 m/s observed. Given the Rossby radius of deformation of the wave $Ro = \sqrt{gH}/f$ for any depth available, whether it be 20 meters depth ($Ro = 201km$ equal to the Texas shelf break at its widest point) or 3000 meters depth ($Ro = 2464km$), is likely too large to only "feel" a 20 m bottom. Additionally, a Kelvin wave needs a "wall like" structure to exist, which in reality is rarely approximated and not found at all on the LATEX shelf.

A fitting of the data to modal structures, as *Church et al.* [1986] has done, may provide a more quantitative analysis for a future study either using Hurricane Andrew, or other more recent observations. The Northwest Gulf particulary invites further investigation due to several unique features of the region that may result in interesting studies or perhaps observational comparison to theory. The Texas shelf features a very sharp bend (nearly 90 degrees) from a zonal to meridional extent towards the south. The evidence in this study shows that trapped waves propagate through the bend and continue south into Mexican waters. The results here were largely qualitative and observational, however a further study could easily examine the evolution of the characteristics (frequency, group and phase speed, and modal structure) of a trapped wave through the bend. *Grimshaw* [1977] investigated several factors including coastline curvature on shelf waves and the LATEX shelf may be a good testbed for such an investigation. Additionally, the eastern portion of the LATEX shelf is near the Mississippi river, one of the largest freshwater outputs in the world and the largest in the United States. This means that a large volume of freshwater flows out and on top of the surrounding coastal waters potentially creating large stratification. Though this study shows that the dominant response is barotropic, the eastern portion certainly has a degree of baroclinic response, as also noted by

KG99. The phenomena of a coastal trapped wave that propagates from a region of high stratification to a region of lower stratification is an interesting one, and provides a possibility of a future study on the effects of variable alongshelf stratification on coastal trapped wave characteristics. Regrettably, mode fitting and propagation through sharply varying topography and varying stratification were beyond the scope of this study, which was to identify the coastal trapped wave response to Hurricane Andrew.

REFERENCES

Adams, J. K., and V. T. Buchwald (1969), The generation of continental shelf waves, *J. Fluid Mech.*, *35*, 815–826.

Allen, J. S. (1975), Coastal trapped waves in a stratified ocean, *J. Phys. Oceanogr.*, *5*, 300–325.

Allen, J. S. (1980), Models of wind-driven currents on the continental shelf, *Annu. Rev. Fluid Mech.*, *12*, 389–433.

Bigelow, H. B., and W. T. Edmondson (1947), *Wind waves at sea; breakers and surf*, 177 pp., U. S. Navy Dept. Hydrographic Office Pub. No. 602, Washington, DC.

Brink, K. H. (1980), Propagation of barotropic continental shelf waves over irregular bottom topography, *J. Phys. Oceanogr.*, *10*(5), 765–778.

Brink, K. H. (1982), A comparison of long coastal trapped wave theory with observations off Peru, *J. Phys. Oceanogr.*, *12*(8), 897–913.

Brink, K. H. (1991), Coastal-trapped waves and wind-driven currents over the continental-shelf, *Annu. Rev. Fluid Mech.*, *23*, 389–412.

Brink, K. H. (2006), Coastal-trapped waves with finite bottom friction, *Dyn. Atmos. Oceans*, *41*(3-4), 172–190.

Brink, K. H., and D. C. Chapman (1987), Programs for computing properties of coastal-trapped waves and wind-driven motions over the continental shelf and slope, *Rep. WHOI-87-24*, 46 pp., Woods Hole Oceanographic Institution, Woods Hole, MA.

Brooks, D. A. (1978), Subtidal sea level fluctuations and their relation to atmospheric forcing along the North Carolina coast, *J. Phys. Oceanogr.*, *8*, 481–493.

Brooks, D. A. (1983), The wake of Hurricane Allen in the western Gulf of Mexico, *J. Phys. Oceanogr.*, *13*(1), 117–129.

Buchwald, V. T., and R. A. D. Szoeke (1973), The response of a continental-shelf to travelling pressure disturbances, *Aust. J. Mar. Freshwater Res.*, *24*(2), 143–58.

Cardone, V. J., and A. T. Cox (1992), Hindcast study of Hurricane Andrew (1992) offshore Gulf of Mexico, 158 pp., Oceanweather Inc., Cos Cob, CT.

Cardone, V. J., A. T. Cox, J. A. Greenwood, D. J. Evans, H. Feldman, S. M. Glenn, and T. R. Keen (1994), Hindcast study of wind wave and currents in Hurricane Andrew, Gulf of Mexico, final report, 476 pp., Minerals Management Service, Herndon, VA.

Church, J. A., H. J. Freeland, and R. L. Smith (1986), Coastal-trapped waves on the east Australian continental shelf part 1: Propagation of modes, *J. Phys. Oceanogr.*, *16*(11), 1929–1943.

Clarke, A. J. (1977), Observational and numerical evidence for wind-forced coastal trapped long waves, *J. Phys. Oceanogr.*, *7*, 231–247.

Cutchin, D. L., and R. L. Smith (1973), Continental shelf waves : Low frequency variations in sea level and currents over the Oregon continental shelf, *J. Phys. Oceanogr.*, *3*, 73–82.

DiMarco, S. F., A. E. Jochens, and M. K. Howard (1997), LATEX shelf data report: Current meter moorings, April 1992 to December 1994, 3701 pp., Texas A&M University Dept. of Oceanography, College Station, TX.

DiMarco, S. F., E. Meza, and J. Zhang (2001), Estimating wave elevation from pressure using second order nonlinear wave-wave interaction theory with applications to Hurricane Andrew, *J. Coast. Res.*, *17*(3), 658–671.

Duchon, C. E. (1979), Lanczos filtering in one and two dimensions, *J. Appl. Meteorol.*, *18*(8), 1016–1022.

Dukhovskoy, D. S., S. L. Morey, and J. J. O'Brien (2008), Generation of baroclinic topographic waves by a tropical cyclone impacting a low-latitude continental shelf, *Cont. Shelf Res.*, *29*, 333–351.

Emery, W. J., and R. E. Thomson (2001), *Data Analysis Methods in Physical Oceanography*, second ed., 638 pp., Elsevier, Amsterdam.

Fandry, C. B., L. M. Leslie, and R. K. Steedman (1984), Kelvin-type coastal surges generated by tropical cyclones, *J. Phys. Oceanogr.*, *14*(3), 582–593.

Freeland, H. J., F. M. Boland, J. A. Church, A. J. Clarke, A. M. G. Forbes, A. Huyer, R. L. Smith, R. Thompson, and N. J. White (1986), The Australian Coastal Experiment: A search for coastal-trapped waves, *J. Phys. Oceanogr.*, *16*(7), 1230–1249.

Gill, A. E. (1982), *Atmosphere-ocean dynamics*, International geophysics series, 662 pp., Academic Press, San Diego.

Gill, A. E., and E. H. Schumann (1974), The generation of long shelf waves by the wind, *J. Phys. Oceanogr.*, *4*(1), 83–90.

Greenspan, H. P. (1956), The generation of edge waves by moving pressure distributions, *J. Fluid Mech.*, *1*(6), 574–592.

Grimshaw, R. (1977), The effects of a variable Coriolis parameter, coastline curvature and variable bottom topography on continental shelf waves, *J. Phys. Oceanogr.*, *7*(4), 547–554.

Grimshaw, R. (1988), Large-scale, low-frequency response on the continental shelf due to localized atmospheric forcing systems, *J. Phys. Oceanogr.*, *18*(12), 1906–1919.

Hamon, B. V. (1962), The spectrums of mean sea level at Sydney, Coff's Harbour, and Lord Howe Island, *J. Geophys. Res.*, *67*(13), 5147–5155.

Hsu, S. A., and Z. Yan (1998), A note on the radius of maximum wind for hurricanes, *J. Coast. Res.*, *14*(2), 667–668.

Huthnance, J. M. (1975), On trapped waves over a continental shelf, *J. Fluid Mech.*, *69*(JUN24), 689–704.

Huthnance, J. M. (1978), Coastal trapped waves: Analysis and numerical calculation by inverse iteration, *J. Phys. Oceanogr.*, *8*(1), 74–92.

Keen, T. R., and S. M. Glenn (1999), Shallow water currents during Hurricane Andrew, *J. Geophys. Res.*, *104*(C10), 23,443–23,458.

Landsea, C. W., J. L. Franklin, C. J. McAdie, J. L. Beven, J. M. Gross, B. R. Jarvinen, R. J. Pasch, E. N. Rappaport, J. P. Dunion, and P. P. Dodge (2004), A reanalysis of Hurricane Andrew's intensity, *Bull. Amer. Meteor. Soc.*, *85*(11), 1699–1712.

LeBlond, P. H., and L. A. Mysak (1978), *Waves in the Ocean*, Elsevier Oceanography Series, 602 pp., Elsevier, Amsterdam.

Liu, Y., X. S. Liang, and R. H. Weisberg (2007), Rectification of the bias in the wavelet power spectrum, *Journal of Atmospheric and Oceanic Technology*, *24*(12), 2093–2102.

Magaard, L., and L. A. Mysak (1986), Ocean waves: classification and basic features, in *Landolt-Brnstein, New Series, Vol. V/3c: Oceanography*, vol. 3c, edited by J. Sndermann, pp. 1–16, Springer-Verlag, Berlin.

Meyers, S. D., B. G. Kelly, and J. J. O'Brien (1993), An introduction to wavelet analysis in oceanography and meteorology: With application to the dispersion of Yanai waves, *Monthly Weather Review*, *121*, 2858–2866.

Mooers, C. N. K., and R. L. Smith (1968), Continental shelf waves off Oregon, *J. Geophys. Res.*, *73*(2), 549–557.

Munk, W., F. Snodgrass, and G. Carrier (1956), Edge waves on the continental shelf, *Science*, *123*(3187), 127–132.

Mysak, L. A. (1967), On the theory of continental shelf waves, *J. Mar. Res.*, *25*(3), 205–227.

Mysak, L. A. (1980), Topographically trapped waves, *Annu. Rev. Fluid Mech.*, *12*, 45–76.

Nowlin, J., W. D., A. E. Jochens, R. O. Reid, and S. F. DiMarco (1998), Texas-Louisiana Shelf Circulation and Transport Processes Study: Synthesis report, Volume I: Technical report, OCS study MMS 98-0035, 502 pp., U.S. Dept. of the Interior, Minerals Management Service, Gulf of Mexico OCS Region, New Orleans, LA.

Palmer, R. (1996), History of coastal engineering in Great Britain, in *History and Heritage of Coastal Engineering*, edited by N. C. Kraus, p. 610, ASCE, New York.

Reid, R. O. (1958), Effect of Coriolis force on edge waves (1) investigation of the normal modes, *J. Mar. Res.*, *16*(2), 109–144.

Robinson, A. R. (1964), Continental shelf waves and the response of sea level to weather systems, *J. Geophys. Res.*, *69*(2), 367–368.

Science Applications International Corporation (1994), Louisiana/Texas shelf physical oceanography program: Eddy circulation study, annual report: Year 1, *OCS Study/MMS 94-0027*, 53 pp., U.S. Department of the Interior, Minerals Management Service, Gulf of Mexico OCS Region, New Orleans, LA.

Smith, R. L. (1978), Poleward propagating perturbations in currents and sea levels along the Peru coast, *J. Geophys. Res.*, *83*(NC12), 6083–6092.

Tang, Y. M., and R. Grimshaw (1995), A modal analysis of coastally trapped waves generated by tropical cyclones, *J. Phys. Oceanogr.*, *25*(7), 1577–1598.

Tang, Y. M., P. Holloway, and R. Grimshaw (1997), A numerical study of the storm surge generated by Tropical Cyclone Jane, *J. Phys. Oceanogr.*, *27*(6), 963–976.

Thiebaut, S., and R. Vennell (2010), Observation of a fast continental shelf wave generated by a storm impacting Newfoundland using wavelet and cross-wavelet analyses, *J. Phys. Oceanogr.*, *40*(2), 417–428.

Thomson, R. E. (1970), On the generation of Kelvin-type waves by atmospheric disturbances, *J. Fluid Mech.*, *42*(4), 657–670.

Thomson, S. W. (1879), On gravitational oscillations of rotating water, *Proceedings of the Royal Society of Edinburgh*, *10*, 92–100.

Torrence, C., and G. P. Compo (1998), A practical guide to wavelet analysis, *Bull. Amer. Meteor. Soc.*, *79*(1), 61–78.

Wang, D. P. (1975), Coastal trapped waves in a baroclinic ocean, *J. Phys. Oceanogr.*, *5*(2), 326–333.

Wang, D. P., and C. N. K. Mooers (1976), Coastal-trapped waves in a continuously stratified ocean, *J. Phys. Oceanogr.*, *6*(6), 853–863.

Wiegel, R. L., and T. Saville Jr. (1996), History of coastal engineering in the USA, in *History and Heritage of Coastal Engineering*, edited by N. C. Kraus, p. 610, ASCE, New York.

Zhang, X., S. F. DiMarco, D. C. Smith IV, M. K. Howard, A. E. Jochens, and R. D. Hetland (2009), Near-resonant ocean response to sea breeze on a stratified continental shelf, *J. Phys. Oceanogr.*, *39*, 2173–2155.

VITA

Stuart Michael Pearce earned his Bachelor of Science degree in Marine Biology with a Physics minor from Auburn University in 2005. In 2006, he entered the Ocean Observing System certificate program and completed the coursework towards a Masters of Geoscience degree, but in 2008 formally continued coursework to earn a Masters of Oceanography in Physical Oceanography in December 2011, resulting in this thesis of study. His interests continue in Ocean Observing Systems and is currently working for the Ocean Observatories Initiative (OOI) at Oregon State University.

Mr. Pearce can be reached by contacting his Texas A&M advisor Dr. Steven DiMarco at Dept. of Oceanography, MS 3146, Texas A&M University, College Station, TX 77843-3146.